

# Mycolactone subverts immunity by selectively blocking the Sec61 translocon

Ludivine Baron<sup>1,7</sup>, Anja Paatero<sup>2,7</sup>, Jean-David Morel<sup>1,7</sup>, Francis Impens<sup>3,†</sup>, Laure Guenin-Macé<sup>1</sup>, Sarah Saint-Auret<sup>4</sup>, Nicolas Blanchard<sup>4</sup>, Rabea Dillmann<sup>2</sup>, Fatoumata Niang<sup>1</sup>, Sandra Pellegrini<sup>5</sup>, Jack Taunton<sup>6</sup>, Ville O Paavilainen<sup>2,8\*</sup>, Caroline Demangel<sup>1,8\*</sup>

<sup>1</sup> *Institut Pasteur, Inserm U1221, Unité d'Immunobiologie de l'Infection, 75015 Paris, France*

<sup>2</sup> *Institute of Biotechnology, University of Helsinki, 00014 Helsinki, Finland*

<sup>3</sup> *Institut Pasteur, Inserm U604, INRA Unité sous-contrat 2020, Unité des Interactions Bactéries-Cellules, 75015 Paris, France*

<sup>4</sup> *Université de Strasbourg, CNRS UMR 7509, ECPM, 67087 Strasbourg, France*

<sup>5</sup> *Institut Pasteur, Inserm U1221, Unité de Signalisation des Cytokines, 75015 Paris, France*

<sup>6</sup> *Department of Cellular and Molecular Pharmacology, University of California San Francisco, CA 94158-2140, USA*

<sup>†</sup> *Present address: Medical Biotechnology Center, VIB, Ghent University, 9000 Ghent, Belgium*

<sup>7</sup> *Co-first authors*

<sup>8</sup> *Co-senior authors*

\*Correspondence: [ville.paavilainen@helsinki.fi](mailto:ville.paavilainen@helsinki.fi) (VOP), [caroline.demangel@pasteur.fr](mailto:caroline.demangel@pasteur.fr) (CD)

**Short caption:** Immunity lost in translocation

**Non-standard abbreviations:** Buruli ulcers (BU), signal recognition particle (SRP), ribosome-nascent polypeptide complex (RNC), stable isotope labeling with amino acids in cell culture (SILAC), ionomycin (IO), gene ontology cellular component (GO\_CC), SwissProt-Protein Information resource (SP-PIR), canine rough microsomes (CRM), liquid chromatography-mass spectrometry (LC-MS), Wiskott Aldrich Syndrome Protein (WASP), Type 2 Angiotensin II Receptor (AT2R), peripheral lymph nodes (PLN).

## ABSTRACT

Mycolactone, an immunosuppressive macrolide released by the human pathogen *Mycobacterium ulcerans*, was previously shown to impair Sec61-dependent protein translocation, but the underlying molecular mechanism was not identified. Here, we show that mycolactone directly targets the alpha subunit of the Sec61 translocon to block the production of secreted and integral membrane proteins with high potency. We identify a single amino acid mutation conferring resistance to mycolactone, which localizes its interaction site near the luminal plug of Sec61 $\alpha$ . Quantitative proteomics reveals that during T cell activation, mycolactone-mediated Sec61 blockade affects a selective subset of secretory proteins including key signal-transmitting receptors and adhesion molecules. Expression of mutant Sec61 $\alpha$  in mycolactone-treated T cells rescued their homing potential and effector functions. Furthermore, when expressed in macrophages the mycolactone-resistant mutant restored IFN- $\gamma$  receptor-mediated anti-microbial responses. Our data thus provide definitive genetic evidence that Sec61 is the host receptor mediating the diverse immunomodulatory effects of mycolactone, and identify Sec61 as a novel regulator of immune cell functions.

## INTRODUCTION

*Mycobacterium ulcerans*, the causative agent of Buruli ulcers (BU), infects and destroys human skin without alerting the host immune system (Demangel et al., 2009). The lack of inflammatory infiltrates in ulcerative lesions is a striking histopathological feature of BU (Guarner et al., 2003). Moreover, BU patients display systemic defects in cellular immune responses, such as a reduced capacity of peripheral blood T cells to produce cytokines upon *ex vivo* stimulation (Phillips et al., 2009). These defects are independent of the activation stimulus and resolve upon treatment of the disease, showing their association with *M. ulcerans*. Bacterial virulence relies on the production of mycolactone, a polyketide-derived macrolide with ulcerative properties in the skin (George et al., 1999). While bacteria remain primarily at the site of infection, mycolactone diffuses into mononuclear blood cells, lymph nodes and spleen (Hong et al., 2008; Sarfo et al., 2011), allowing it to exert immunosuppressive effects at the systemic level. Intraperitoneal delivery of mycolactone protects mice against chemically-induced skin inflammation (Guenin-Mace et al., 2015). It prevents peripheral blood lymphocyte homing to draining lymph nodes and expansion upon antigenic stimulation (Guenin-Mace et al., 2011). Finally, *M. ulcerans* strains deficient for mycolactone production do not induce functional defects in peripheral blood T cells of infected mice (Hong et al., 2008). Therefore, mycolactone has the intrinsic capacity to block the development of innate and adaptive immune responses *in vivo*.

*In vitro* mycolactone blunts the capacity of immune cells to produce selected cytokines, chemokines and homing receptors without inducing cellular stress or cytotoxicity (Hall and Simmonds, 2014). Mycolactone operates post-transcriptionally and independently of mTOR, and as such represents a novel type of natural immunosuppressor. Hall *et al.* showed that mycolactone blocks the translocation of inflammatory mediators (TNF- $\alpha$  and Cox2) as well as model secretory proteins into the endoplasmic reticulum (ER), with subsequent degradation of these proteins by the ubiquitin:proteasome system (Hall et al., 2014). Using cell-free systems, McKenna *et al.* later identified the translocation stage that mycolactone inhibits, and highlighted differences in mycolactone-mediated inhibition of cotranslationally versus post-translationally inserted Sec61 secretory substrates (McKenna et al., 2016). In eukaryotes, cotranslational protein translocation is initiated by recognition of signal peptides or

nascent polypeptide anchor domains by the signal recognition particle (SRP). The SRP then targets the ribosome-nascent polypeptide complex (RNC) to the Sec61 translocon for insertion into the ER lumen (Park and Rapoport, 2012). McKenna *et al.* provided biochemical evidence that mycolactone induces a conformational change in the pore-forming subunit of the translocon, Sec61 $\alpha$  (McKenna *et al.*, 2016). While Sec61, SRP-receptor and SRP are sufficient for minimal translocation to occur, accessory components such as Sec62/63, TRAM, TRAP complex, and BiP facilitate the process. What is the precise molecular target of mycolactone, and how mycolactone's ability to prevent protein translocation connects with reduced cellular immune responses remained critical open questions.

## RESULTS

### **Mycolactone targets the Sec61 translocon**

Amongst known inhibitors of protein translocation, three have been formally shown to act by directly targeting Sec61 $\alpha$ : the cyclic heptadepsipeptide HUN-7293/cotransin/CT8, decadepsipeptide decatransin and cyanobacterial product apratoxin A (Garrison *et al.*, 2005; Junne *et al.*, 2015; Mackinnon *et al.*, 2014; Maifeld *et al.*, 2011; Paatero *et al.*, 2016). All of these drugs target a partially overlapping site in the pore-forming Sec61 $\alpha$  subunit. However, unlike decatransin and apratoxin A, CT8 inhibits Sec61 in a substrate-selective manner. To test the hypothesis that mycolactone and CT8 use similar mechanisms of action, we performed competitive Sec61 $\alpha$  binding assays with a structural variant of CT8 that covalently cross-links to Sec61 $\alpha$  upon photoactivation (MacKinnon *et al.*, 2007; Mackinnon *et al.*, 2014) (Fig. S1A). ER microsomes were incubated with CT7 in the presence or absence of increasing amounts of mycolactone, then photolysed and denatured. The presence of CT7 cross-linked to Sec61 $\alpha$  was then quantitatively assessed by click-chemistry and in-gel fluorescent scanning. Mycolactone competed dose-dependently with CT7 for binding to Sec61 $\alpha$  (Fig. 1A), similarly as the potent cotransin analog CT9 (Fig. 1B, Fig. S1A). Importantly, mycolactone displaced CT7 slightly more efficiently than CT9, indicating that it binds Sec61 $\alpha$  with comparable or higher affinity and may share a coinciding binding site on Sec61 $\alpha$ .

Mycolactone consists of a lactone ring and two polyketide chains branched in the north and south positions (Fig. S1A). We reported previously that variant 5b lacking the northern side-chain partially retains the immunosuppressive activity of mycolactone, whereas subunits lacking the southern or both side chains (4a and 5a, respectively) are biologically inert (Guenin-Mace et al., 2015). Consistently, 5b competed with CT7 with approximately 10-fold reduced potency, whereas 4a and 5a showed no competitive activity (Fig. 1C). No difference in ability of mycolactone to compete with CT7 for Sec61 $\alpha$  binding was observed after extensive washing of microsomes (Fig. 1D), indicating that mycolactone binds tightly to the translocon, and has a slow dissociation rate.

A previous genetic screen identified several point mutations in Sec61 $\alpha$  (R66I, R66G, S82P, M136T) that reduce CT8 binding without major effects on channel function (Mackinnon et al., 2014). Given that mycolactone and CT8 likely have overlapping binding sites, we tested whether these mutations confer resistance to mycolactone. For this purpose, we treated HEK293-FRT cells over-expressing wild-type (wt) or mutant Sec61 $\alpha$  constructs with increasing concentrations of mycolactone. The viability of cells expressing wt-Sec61 $\alpha$  was potently reduced by mycolactone ( $IC_{50}$  = 10 nM) (Fig. 1E). In contrast, cells expressing the R66I, R66G and S82P mutant alleles were highly desensitized ( $IC_{50}$  > 1000 nM). Interestingly, these mutations cluster near the luminal plug of Sec61 $\alpha$  (Fig. S1B), suggesting that this region forms the mycolactone interaction site. This finding was fully consistent with McKenna et al's observation that mycolactone alters protease sensitivity of Sec61 $\alpha$  *in vitro* (McKenna et al., 2016). Focusing on the R66G construct, we investigated whether this single amino acid mutation confers resistance to mycolactone-mediated blockade of protein secretion. HEK293-FRT cells stably expressing wt or R66G-Sec61 $\alpha$  were transfected with a secreted Gaussia luciferase construct, then subjected to a 24h mycolactone treatment that did not alter cell viability. While mycolactone efficiently blocked luciferase secretion in cells expressing wt-Sec61 $\alpha$  ( $IC_{50}$  = 3 nM), cells expressing the R66G-Sec61 $\alpha$  mutant proved highly resistant ( $IC_{50}$  > 1000 nM) (Fig. 1F). In addition to providing additional evidence that mycolactone binds to Sec61 $\alpha$ , these data revealed the critical importance of the Sec61 $\alpha$  R66 residue for mycolactone's inhibitory activity on protein translocation.

## **Mycolactone is a broad-spectrum inhibitor of Sec61**

A distinguishing feature of CT8 is its ability to prevent the translocation of only a minor subset of Sec61 clients (Besemer et al., 2005; Garrison et al., 2005; Maifeld et al., 2011). To determine if mycolactone shares this property, we compared the effects of mycolactone and CT8 on the production of known Sec61 clients by human immune cells (namely TNF- $\alpha$  production by monocyte-derived macrophages, and interferon (IFN)- $\gamma$ , interleukin-2 and L-selectin production by peripheral blood-derived CD4<sup>+</sup> T cells). Cotransin showed a highly variable inhibitory activity towards the different substrates (IC<sub>50</sub> between 20 and 1050 nM) (data not shown). In contrast, mycolactone prevented the production of all tested proteins with IC<sub>50</sub> between 4.5 and 12 nM, suggesting that it is a more potent and less selective Sec61 inhibitor. We next used global proteome analysis of SILAC-labeled T cells to gain a broader view of mycolactone activity, and identify the proteins impacted by Sec61 inhibition during T cell activation. Jurkat T cells were grown in light or heavy SILAC medium for five cell divisions then treated with 40 nM mycolactone or vehicle for 1h prior to activation with phorbol myristate acetate (PMA) and ionomycin (IO) for 6h. These conditions induced full cell activation, bypassing a potential inhibitory effect of mycolactone on TCR expression (Boulikroun et al., 2010). Cells were then lysed and equal amounts of light- and heavy-labeled protein extracts were mixed. Proteins were trypsin-digested and peptide mixtures analyzed by LC-MS/MS. The SILAC analysis was repeated with reversed labeling conditions, allowing the reliable identification and quantification of 6,503 proteins (hereafter referred to as “identified proteins”). Among these, 4,636 proteins were quantified in both labeling conditions. SILAC analyses were performed on cell extracts, and consequently most secreted proteins were not detected. Notably, 52 proteins were consistently downregulated in mycolactone-treated cells ( $\log_2$  mycolactone/control ratio <-0.5), while only 2 proteins (putative E3 ubiquitin-protein ligase LRRCS8 and Hsp70 chaperone HSPA1A) were upregulated ( $\log_2$  mycolactone/control ratio >0.5) (Fig. 2A, Table S1). Figure 2B compares the distribution of “mycolactone-downregulated”, “identified” and “all human” proteins across the different subcellular compartments. In contrast to cytoplasmic and nuclear proteins, the incidence of plasma membrane and ER located proteins was increased in “mycolactone-downregulated” proteins, compared to “identified” proteins (Fig. 2B), indicating a selective

downregulation of these proteins by mycolactone. A key word analysis confirmed this observation and revealed an additional enrichment in glycoproteins, immunoglobulin domain-containing proteins and proteins involved in the immune response among “mycolactone-downregulated” proteins (Fig. 2C).

Consistent with Sec61 inhibition, 42 of the 52 mycolactone-downregulated proteins contained a signal sequence or transmembrane domain directing newly synthesized proteins to the translocon (Table S1). The mycolactone-downregulated subset was significantly enriched in single-pass type I/II membrane proteins (Fig. 2D), indicating that such proteins are particularly susceptible to Sec61 inhibition by mycolactone. In contrast, the incidence of multi-pass membrane proteins was comparable between “downregulated proteins” and “identified proteins”, suggesting that some multi-pass membrane proteins may bypass mycolactone-mediated blockade of Sec61. To test this hypothesis, mRNAs for various Sec61 substrates were translated in a reconstituted mammalian translation system in the presence of canine rough microsomes (CRM), <sup>35</sup>S-methionine and increasing concentrations of mycolactone. In accordance with previously reported *in vitro* translation (IVT) assays of Sec61-dependent secretory and type II transmembrane protein TNF- $\alpha$  (Hall et al., 2014; McKenna et al., 2016), ER translocation of secreted prolactin and IFN- $\gamma$  was efficiently and dose-dependently suppressed by mycolactone (Fig. 2E, Fig. S1C). Translocation of ER-resident binding immunoglobulin protein BiP (also known as HSPA5) was also affected, confirming the SILAC data (Fig. 2E, Table S1). BiP being a critical mediator of Sec61-dependent translocation, its depletion may contribute indirectly to the defective biogenesis of Sec61 clients in mycolactone-exposed cells. Multi-pass membrane proteins Mucolipin-1 (Mcln) and a synthetic multi-pass membrane protein derived from *E.coli* leader peptidase (LEP) (Lundin et al., 2008) were also susceptible to mycolactone in IVT assays. In contrast, the multi-pass ER membrane protein CIG30 (Monne et al., 1999) was consistently resistant to mycolactone concentrations up to 1  $\mu$ M (Fig. 2E, Fig. S1C). The SILAC and *in vitro* assays of protein translocation are thus fully consistent with mycolactone being a broad-acting inhibitor of Sec61 client production, with a more selective activity on multi-pass membrane proteins.

### **Sec61 blockade affects IFN- $\gamma$ signaling in Jurkat T cells**

Among the 52 proteins found to be downregulated by mycolactone in PMA/IO-stimulated Jurkat T cells, 10 did not contain a signal sequence or transmembrane domain identifying them as a Sec61 client (Table S1). They were all encoded by IFN-stimulated genes (9 by IFN- $\gamma$  and 1 by IFN- $\alpha$ ), leading us to examine the effects of mycolactone on both the production of IFNs and the cell's response to exogenous IFNs. Consistent with previous reports, exposing Jurkat T cells to mycolactone for 1h before PMA/IO activation efficiently prevented IFN- $\gamma$  production (Fig. 3A), despite robust *IFN- $\gamma$*  mRNA induction (Fig. 3B). Moreover, mycolactone-treated cells rapidly lost the ability to respond to IFN- $\gamma$ : T cells exposed to mycolactone for more than 20 min prior to 20 min stimulation with IFN- $\gamma$  showed reduced STAT1 phosphorylation (Fig. 3C). The IFN- $\gamma$  receptor (IFNGR) was not detected by our SILAC analysis, likely because protein level was below the detection limit. Yet, using flow cytometry we found that a 6h exposure to mycolactone led to a 60% reduction in T cell surface expression of IFNGR1 (Fig. 3D). Since the level of *IFNGR1* transcripts was not altered in mycolactone-treated cells (Fig. 3E), the loss of IFNGR1 likely results from Sec61 blockade. We conclude that both the reduced IFN- $\gamma$  production and the loss of IFNGR1 impair the IFN- $\gamma$  autocrine loop in PMA/IO-activated T cells exposed to mycolactone. This was further evidenced by the reduced accumulation of the IFN- $\gamma$ -inducible GBP2 at the mRNA level (Fig. 3F), and a Western blot analysis validating our SILAC observation that mycolactone downregulates GBP2 protein levels in activated Jurkat T cells (Fig. 3G, Table S1). We also measured T cell responses to IFN- $\alpha$ . In Jurkat T cells exposed for 6h to mycolactone, the surface level of the type I IFN receptor subunits (IFNAR1 and IFNAR2) was also reduced, but to a lesser extent than IFNGR1 (Fig. 3D). Consistently, phosphorylation of STAT1/3 was barely affected in T cells exposed to mycolactone for 6h then pulsed with IFN- $\alpha$  for 20 min. However, after a 24h-exposure, IFN- $\alpha$  signaling declined considerably (Fig. 3H). Altogether, our SILAC data show that the magnitude and kinetics of mycolactone effects vary between Sec61 substrates, likely reflecting differences in protein turnover rates.

### **The R66G mutation in Sec61 $\alpha$ confers broad resistance to mycolactone**

Production of IFN- $\gamma$  by T cells and IFN- $\gamma$ -induced expression of nitric oxide synthase (iNOS) in infected macrophages are both essential for control of mycobacterial infection (Flynn and Chan, 2001). *M.*

*ulcerans* is no exception, as shown by the reduced capacity of IFN- $\gamma$  knock-out mice to kill intracellular bacilli during the early intra-macrophage growth phase of the bacteria (Bieri et al., 2016). To evaluate the contribution of Sec61 to mycolactone virulence, we examined whether mycolactone-resistant Sec61 mutants rescued the generation of anti-mycobacterial immune responses. Primary T cells isolated from mouse lymphoid organs were transduced with retroviral vectors for over-expression of wt- or R66G-Sec61 $\alpha$ , and fluorescent reporter protein Zsgreen (Fig. 4A). Non-transduced and wt-Sec61 $\alpha$ -transduced cells were equally susceptible to mycolactone treatment, as demonstrated by the comparable inhibition of CD4 expression in mycolactone-exposed Zsgreen<sup>+</sup> and Zsgreen<sup>-</sup> cells (Fig. 4B). Strikingly, expression of R66G-Sec61 $\alpha$  conferred resistance to mycolactone-induced defects in CD4 expression (Fig. 4B). We reported previously that mycolactone efficiently down-regulates the expression of CD62L at the surface of naïve T cells (Guenin-Mace et al., 2011). Similar to CD4, CD62L expression resisted mycolactone treatment in T cells expressing R66G-Sec61 $\alpha$ , but not wt-Sec61 $\alpha$  (Fig. 4C). Further, in T cells transduced with R66G-Sec61 $\alpha$  and stimulated with PMA/IO, the production of IFN- $\gamma$  was unaffected by mycolactone treatment (Fig. 4D). This demonstrated that defects in cytokine production are also fully corrected by expression of R66G-Sec61 $\alpha$ . A similar approach was used to assess the functional impact of Sec61 inhibition in macrophages (Fig. 4E). Transduction of R66G-Sec61 $\alpha$ , but not wt-Sec61 $\alpha$ , in bone marrow-derived macrophages conferred resistance to mycolactone-mediated inhibition of IFNGR1 expression (Fig. 4F). This re-established the bactericidal capacity of macrophages, as LPS+IFN- $\gamma$ -driven production of iNOS was restored in macrophages expressing R66G- but not wt-Sec61 $\alpha$  (Fig. 4G). By inhibiting Sec61 activity, mycolactone thus prevents both IFN- $\gamma$  production by T cells and macrophage responsiveness to IFN- $\gamma$ -stimulation.

### **Mycolactone suppresses Sec61 activity in T cells *in vivo***

Data in Figure 4C show that CD62L expression by mouse primary T cells is highly susceptible to mycolactone-induced inhibition of Sec61. Using this membrane receptor as a read-out, we next investigated whether systemically-delivered mycolactone impacts Sec61 activity in adoptively transferred T cells. Because mycolactone-induced loss of CD62L impairs T cell capacity to reach

peripheral lymph nodes (PLN) (Guenin-Mace et al., 2011), we also examined if Sec61 blockade results in impaired homing properties. Primary T cells isolated from wild-type (C57BL/6J, CD45.2<sup>+</sup>) and congenic CD45.1 mice were transduced with wt- or R66G-Sec61 $\alpha$  (Fig. 5A). CD45.2<sup>+</sup> wt-Sec61 $\alpha$  transduced cells were then mixed with CD45.1<sup>+</sup> R66G-Sec61 $\alpha$  transduced cells in equal proportions, and vice-versa. Each mix of cells was then injected intravenously into wild-type recipient mice. Concomitantly, mice were given an intraperitoneal injection of mycolactone (1 mg/kg), a treatment previously shown to induce anti-inflammatory effects *in vivo* (Guenin-Mace et al., 2015). After 24 hours, the mean surface expression of CD62L and the relative proportions of wt- and R66G-Sec61 $\alpha$  transduced cells in PLN and spleen were determined by FACS analysis. In mycolactone-injected mice, the expression of CD62L was reduced in wt-, but not R66G-Sec61 $\alpha$  transduced T cells from the spleen (Fig. 5B, left). A similar trend was observed in T cells from PLN (Fig. 5B, right). This experiment demonstrated that mycolactone modulates T cell expression of CD62L *in vivo*, in a Sec61-dependent manner. Notably, R66G-Sec61 $\alpha$  transduced T cells were recovered from PLN at significantly higher frequencies than wt-Sec61 $\alpha$  transduced T cells (Fig. 5C, right). These frequencies were instead comparable in the spleen, consistent with CD62L not being critical for T cell homing to this organ (Fig. 5C, left). Therefore, mycolactone down-regulates both Sec61-dependent expression of CD62L and CD62L-dependent lymphocyte homing *in vivo*.

In conclusion, we have shown that mycolactone-induced Sec61 blockade is due to a direct interaction with Sec61 $\alpha$ , which determines mycolactone's ability to prevent the generation of innate and adaptive immune responses. These data provide a molecular explanation for the immunological defects of BU patients. More generally, they highlight the critical importance of Sec61 activity for immune cell function, migration and communication. Compared to CT8, mycolactone was more cytotoxic in human primary dermal fibroblasts, and equally poorly cytotoxic in Jurkat T cells (Fig. S2A). It was more effective than CT8 at inhibiting the production of cytokines and homing receptors by immune cells, and our ongoing investigations suggest that mycolactone is also more potent than Apratoxin A in these bioassays (data not shown). Among known inhibitors of Sec61, mycolactone is therefore the first produced by a human pathogen and likely the most potent.

Mycolactone was previously reported to bind and activate N-WASP and AT2R to mediate skin ulceration and analgesia, respectively (Guenin-Mace et al., 2013; Marion et al., 2014). Silencing of N-WASP/WASP or AT2R in relevant cell models did not modify the inhibitory effect of mycolactone on the production of secreted and membrane proteins (Fig. S2B-C), showing that the immunomodulatory properties of mycolactone are independent of these proteins. It is nevertheless possible that Sec61 inhibition mediates, or at least contributes to the ulcerative and analgesic properties of mycolactone initially attributed to N-WASP and AT2R, respectively.

Altogether, our data reveal a novel mechanism of immune evasion evolved by pathogenic mycobacteria, which targets host cell protein translocation. Inhibition of Sec61 activity efficiently prevented the production of key mediators of innate and adaptive immune responses against intracellular pathogens, as we demonstrated for IFN- $\gamma$  and IFN- $\gamma$  receptor. The discovery that mycolactone inhibits Sec61 opens novel perspectives, beyond the field of inflammation. Since CT8 was effective at limiting proteostasis of enveloped viruses (Heaton et al., 2016), mycolactone may similarly show broad anti-viral activity. It may also prove useful in the treatment of pathologies associated with elevated secretory protein synthesis. Genetically modifying Sec61 demonstrated the specificity of mycolactone binding to the translocon. Since Sec61 clients are expressed in a cell-type specific manner, mycolactone-mediated inhibition of protein translocation into the ER could underpin the variety of its effects in different cell type, and the distinctive features of BU.

## **MATERIALS and METHODS**

**Reagents and expression vectors.** All experiments using mycolactone were done with natural mycolactone A/B purified from *M. ulcerans* bacteria (strain 1615, ATCC 35840), then quantified by spectrophotometry ( $\lambda_{\max}$ =362 nm; log  $\epsilon$ =4.29) (Spangenberg and Kishi, 2010). Synthetic modules of mycolactone (4a, 4b and 5b) were generated as described (Chany et al., 2011). Stock solutions were prepared in either ethanol or DMSO, then diluted 1000x in culture medium for cellular assays or 10x in phosphate buffered saline (PBS) before injection in mice. CT7, CT8 and CT9 were prepared as previously

described (MacKinnon et al., 2007; Maifeld et al., 2011). Sec61 wt or mutant sequences were cloned upstream of an internal ribosome entry site (IRES) of the pRetroX-IRES-ZsGreen retroviral vector (Clontech), for simultaneous translation of Sec61 $\alpha$  and ZsGreen in mouse primary T cells and macrophages.

**SDS-PAGE, autoradiography and Western blotting.** Cell lysates were resolved on NuPAGE Bis-Tris gels and transferred to nitrocellulose membranes (Life Technologies). For autoradiography, dried Tris-tricine gels were exposed to a storage phosphorus screen (GE Healthcare) and imaged on a Typhoon Trio phosphorimager (GE Healthcare). Protein detections used the following antibodies: WASP F-8 (sc-365859, SantaCruz Biotechnology), N-WASP 30D10 (#4848, Cell Signaling), pSTAT1 Y701 (#9171L, Cell Signaling), pSTAT2 Y689 (#07-224, Millipore), pSTAT3 Y705 (#9131L, Cell Signaling), STAT1 (#06-501, Millipore), STAT2 (#06-502, Upstate Millipore), STAT3 (sc-7179, Santa Cruz), AT2R (sc-9040, Santa Cruz),  $\alpha$ -actin (#3700, Cell Signaling) and GAPDH (#2118, Cell Signaling), Sec61 $\alpha$  (NB120-15575, Novus Biologicals). Here, complexes were revealed with the ECL Prime detection reagent (GE Healthcare) and chemiluminescence reading on a Fuji LAS-4000 Luminescent Image Analyzer.

**Photo-affinity labeling.** Protocols for CRM preparation and CT7 photo-affinity labeling and click chemistry were described previously (MacKinnon et al., 2007; Walter and Blobel, 1983). In brief, CRM equivalent to 100 nM Sec61 were treated with 1 or 10  $\mu$ M mycolactone or DMSO for 30 min at 0°C, followed by incubation with 100 nM CT7 for 10 min at room temperature. Samples were then photolyzed for 10 min and crosslinked proteins were detected by click chemistry, SDS-PAGE, and in-gel fluorescence scanning. In Fig. 1D, 50  $\mu$ l photo-affinity labeling reactions were treated with 10  $\mu$ M mycolactone on ice before (pre-) or after (post-) three rounds of membrane pelleting. A third sample was treated post-pelleting with an equal volume DMSO. All the samples were further incubated for 30 min on ice. CT7 crosslinking and click chemistry were then performed as described above.

**IVT assays.** Protein translocation assays were performed as described in (Sharma et al., 2010): DNA templates encoding indicated constructs were transcribed with T7 or SP6 Polymerase (New England Biolabs) for 1-2 h at 37°C and used in subsequent translation/translocation reactions. The reactions were assembled at 0°C in the presence of mycolactone or an equivalent volume of solvent. Reactions included

<sup>35</sup>S-Methionine (Perkin Elmer, 2 µCi per 10 µL translation), and CRM. The amount of CRM was optimized to be 0.25 µl per 10 µl reaction volume. Translation was initiated by transferring the reactions to 32°C for 30 or 60 min and stopped by returning reactions onto ice. Translocation of non-glycosylated proteins was assessed by treating the samples with proteinase K for 1 h at 0°C. An aliquot was incubated in the presence of TX-100 to demonstrate the protection by CRM. Proteinase digestion was stopped with PMSF and boiling in the presence of SDS. After TCA precipitation the remaining, protected proteins/protein fragments were analyzed with SDS-PAGE and autoradiography. The translocation of glycosylated proteins was analyzed by SDS-PAGE and autoradiography. Alternatively, the control samples were first denatured and treated with endoglycosidase H to demonstrate that differences in gel migration are based on glycosylation.

**Cell cultures.** Jurkat T cells (E6.1 clone, ECACC#88042803), HeLa cells (ECACC#93021013), human primary dermal fibroblasts (Life Technologies, C-013-5C) and HEK293-FRT TRex cells stably expressing wt or mutant Sec61α were cultured in RPMI GlutaMAX™ (Jurkat) or DMEM GlutaMAX™ (other cells), from Life Technologies, supplemented with 10% heat-inactivated fetal calf serum (FCS) (Invitrogen), penicillin (100 U/ml) and streptomycin (100 µg/ml)). Human primary T cells were isolated from blood donors by Ficoll density gradient centrifugation and CD4<sup>+</sup> T cell purification by negative depletion (Miltenyi Biotec). Human primary macrophages were obtained from peripheral blood-derived monocytes, isolated by adhesion to tissue culture plastic-ware and cultured with 10 ng/ml human GM-CSF (Peprotech) for 7-12 days. Mouse CD3<sup>+</sup> primary T cells isolated from spleens and lymph nodes by negative selection using the Pan T cell Isolation kit (Miltenyi Biotec), then placed in RPMI supplemented with 10% heat-inactivated FCS, 10 mM Hepes, 1 mM pyruvate and 25 µM 2-mercaptoethanol. Bone marrow-derived macrophages were obtained by a 7-day differentiation of mouse progenitors in DMEM supplemented with 20% heat-inactivated horse serum (Gibco) and 30% L929-conditioned medium as a source of M-CSF.

**SILAC labeling and LC-MS/MS analysis.** For SILAC labeling, Jurkat T cells were cultured in DMEM medium without L-lysine, L-arginine, or L-glutamine (Silantes GmbH) supplemented with 10% heat-inactivated FCS (Invitrogen), 2 mM GlutaMAX and either natural L-arginine HCl and L-lysine HCl (light labeling) (Sigma) or <sup>13</sup>C<sub>6</sub><sup>15</sup>N<sub>2</sub> L-lysine HCl and <sup>13</sup>C<sub>6</sub> L-arginine HCl (heavy labeling) (Silantes GmbH). L-Lysine HCl was added at

its normal concentration in DMEM (146 mg/L), but the concentration of L-arginine HCl was reduced to 30 mg/l (36% of the normal concentration in DMEM) to prevent metabolic conversion of arginine to proline. Cells were kept for at least six population doublings to ensure complete incorporation of the labeled lysine and arginine. Light (L) and heavy (H) SILAC labeled Jurkat T cells were treated with 40 nM mycolactone or vehicle as control for 1h, then activated with PMA/IO for 6h. Two experiments were performed in reverse labeling conditions, yielding four samples. From each condition,  $5.10^6$  cells were harvested, washed twice with PBS and cell pellets were frozen at  $-80^{\circ}\text{C}$  until further use. Each pellet was resuspended in 500  $\mu\text{L}$  lysis buffer (9 M urea in 20 HEPES mM HEPES pH 8.0), sonicated (three bursts of 15" at an amplitude of 20%) and centrifuged for 15' at 16,000xg at  $4^{\circ}\text{C}$  to remove insoluble material. The protein concentration in the supernatants was measured using a Bradford assay (Biorad) and equal protein amounts of mycolactone treated and untreated cell lysates were mixed to obtain two replicate samples with reversed SILAC labeling for further analysis, each containing 5.6 mg total protein (sample 1: vehicle (H) + mycolactone (L); sample 2: vehicle (L) + mycolactone (H)). Proteins in each sample were reduced with 5 mM DTT and incubation for 30 minutes at  $30^{\circ}\text{C}$  and then alkylated by addition of 100 mM chloroacetamide for 15 minutes at room temperature in the dark. Both samples were further diluted with 20 mM HEPES pH 8.0 to a final urea concentration of 2 M and proteins were digested with 50  $\mu\text{g}$  trypsin (Promega) (1/113, w/w) overnight at  $37^{\circ}\text{C}$ . Peptides were then purified on a Sep-Pak C18 cartridge (Waters) and 500  $\mu\text{g}$  peptides of each sample was re-dissolved in 10 mM ammonium acetate pH 5.5 in water/acetonitrile (98/2, vol/vol) and injected on a capillary RP-HPLC column (Zorbax 300SB-C18, 2.1 mm internal diameter, 150 mm length, Agilent Technologies) using a Agilent 1200 Series HPLC system. Peptides were separated by a linear gradient of acetonitrile (from 2% to 70% in 100 min, in 10 mM ammonium acetate pH 5.5) and peptides that eluted between 20 and 92 min were collected in 72 fractions of 1 min each. Fractions with 12 min difference in retention time were pooled to obtain total of 12 fractions for LC-MS/MS per sample. Peptides in each fraction were dried and re-dissolved in 12  $\mu\text{l}$  solvent A (0.1% formic acid in water/acetonitrile (98:2, v/v)) of which 5  $\mu\text{l}$  was injected for LC-MS/MS analysis on an Ultimate 3000 RSLCnano System (Dionex, Thermo Fisher Scientific) in line connected to a Q Exactive mass spectrometer with a Nanospray Flex Ion source (Thermo Fisher Scientific). Trapping was

performed at 10  $\mu$ l/min for 3 min in solvent A on a PepMap<sup>TM</sup> C18 column (0.3 mm inner diameter  $\times$  5 mm (Dionex)) and following back-flushing from the trapping column, the sample was loaded on a reverse-phase column (made in-house, 75  $\mu$ m I.D.  $\times$  500 mm, 1.9  $\mu$ m beads C18 Repronil-Pur, Dr. Maisch). Peptides were eluted by an increase in solvent B (0.08% formic acid in water/acetonitrile (2:8, v/v)) in linear gradients from 5% to 20% in 47 minutes, then from 20% to 40% in 150 minutes and finally from 40% to 55% in 30 minutes, all at a constant flow rate of 300 nl/min. The mass spectrometer was operated in data-dependent mode, automatically switching between MS and MS/MS acquisition for the fifteen most abundant ion peaks per MS spectrum. Full-scan MS spectra (300-2000 m/z) were acquired at a resolution of 70,000 after accumulation to a target value of 1,000,000 with a maximum fill time of 100 ms. The fifteen most intense ions above a threshold value of 100,000 were isolated (window of 2.5 Th) for fragmentation by CID at a normalized collision energy of 27% after filling the trap at a target value of 100,000 for maximum 160 ms with an underfill ratio of 0.1%. The S-lens RF level was set at 55 and we excluded precursor ions with single, unassigned and charge states above six from fragmentation selection.

**Data Processing and Gene Ontology Terms Enrichment Analysis.** Data analysis was performed with MaxQuant (version 1.4.1.2) (Cox and Mann, 2008) using the Andromeda search engine (Cox et al., 2011) with default search settings including a false discovery rate set at 1% on both the peptide and protein level. Spectra were searched against the human proteins in the Uniprot/Swiss-Prot database (database release version of January 2014 containing 20,272 human protein sequences, [www.uniprot.org](http://www.uniprot.org)) with a mass tolerance for precursor and fragment ions of 4.5 and 20 ppm, respectively, during the main search. To enable the identification of SILAC labeled peptides the multiplicity was set to two with Lys8 and Arg6 settings in the heavy channel, allowing for a maximum of 3 labeled amino acids per peptide. Enzyme specificity was set as C-terminal to arginine and lysine, also allowing cleavage at proline bonds and a maximum of two missed cleavages. Variable modifications were set to oxidation of methionine residues and acetylation of protein N-termini. Carbamidomethyl formation of cysteine residues was set as a fixed modification. In total, 6503 proteins were identified in both samples of which 4636 proteins were quantified. For each quantified protein the  $\log_2$  values of the normalized mycolactone/untreated ratio in

both samples were plotted against each other to generate the scatter plot depicted in Figure 2 and Table S1. Proteins with  $\log_2(\text{mycolactone/untreated ratios}) < -0.5$  in both samples were considered as specific mycolactone targets that are downregulated upon treatment. Proteomic data were deposited to the ProteomeXchange Consortium via the PRIDE partner repository with the dataset identifier PXD002971 (Username: reviewer82182@ebi.ac.uk, Password: fUjRaVcG). Gene Ontology and SP-PIR terms enrichment analyses were performed using Database for Annotation, Visualization and Integrated Discovery (DAVID) bioinformatics resources (Huang et al., 2009). Information on the topology of membrane proteins were retrieved from the Uniprot/Swiss-Prot database.

**Flow cytometry.** Staining of mouse cells was performed using anti-CD4 (#553051, BD), anti-CD62L (L-selectin, #553162, BD), anti-CD3 (#553064, BD), anti-CD19 (#550992, BD), anti-CD45.1 (#5061788, BD), anti-IFNGR1 (130-104-988, Miltenyi), anti-IFN- $\gamma$  (#554412, BD) and anti-IL-2 (#554429, BD). For intracellular staining of cytokines, cells were treated with mycolactone for 1h then activated with PMA/IO. GolgiStop (BD Biosciences) was added 2h later. After 6h, cells were fixed with 4% (w/v) paraformaldehyde during 20 min at RT then stained with PE-conjugated anti-IFN- $\gamma$  antibodies (BD Biosciences) in 100  $\mu$ l of PBS + 0.1% BSA + 0.5% saponin for 30 min at RT. For intracellular staining of iNOS, macrophages were fixed with BD Lyse/Fix solution (#558049) for 10min at 37°C then permeabilised with BD Perm Buffer III (#558050) for 20 minutes at 4°C. Staining was performed with goat anti-NOS2 (sc-650-G, Santa Cruz) followed by an anti-goat secondary antibody (#96938, Abcam). Staining of Jurkat was performed using anti-IFNGR1 (#558937, BD), IFNAR1 (#550331, BD) and IFNAR2 (#1080-08, SouthernBiotech). Briefly, human cells were stained with IFNAR1 or IFNAR2, washed twice with PBS, incubated with biotin conjugated rat anti mouse IgG (# 415-065-166, Jackson ImmunoResearch), washed and then incubated with R-Phycoerythrin-conjugated streptavidin (PNIM0557, Beckman Coulter). All FACS acquisition was performed on a BD FACS Accuri C6 and data analysed using FlowJo software.

**Retroviral transduction.** Platinum-E ecotropic packaging cells (platE, Biolabs) transfected with pRetroX-IRES-ZsGreen plasmids containing Sec61 $\alpha$  sequences were used to produce retroviral particles. Immediately after isolation from mouse organs, CD3<sup>+</sup> T cells were activated with Dynabeads<sup>®</sup> Mouse T-activator CD3/CD28 (Miltenyi Biotec) with 1 bead/cell in in RPMI supplemented with 10% heat-

inactivated FCS, 10 mM Hepes, 1 mM pyruvate and 25  $\mu$ M 2-mercaptoethanol (complete medium, CM). Twenty-four hours later, cells were centrifuged at 1200 rpm and the supernatant (conditioned medium) was saved. Cells were resuspended at  $4 \times 10^6$  cells/ml in viral supernatant freshly collected from platE cells and supplemented with 10 $\mu$ g/ml Polybrene (Millipore), distributed at 1 ml/well in a 6-well plate and spin-infected for 1h at 2800 rpm, 32°C. Cell supernatant was then removed and replaced with conditioned medium. After 48h, spin-infection was repeated and T cells were resuspended in CM containing 50% conditioned medium. Bone marrow-derived macrophages were plated in 12 or 24-well plates (2-4.10<sup>5</sup>cells/well) for 20h. Fresh viral supernatant collected from platE cells and 10 $\mu$ g/ml polybrene were added before spin-infection for 1 hour at 2800 rpm, 32°C. Cell supernatant was then removed and replaced with fresh DMEM supplemented with 20% horse serum.

**Bioassays.** The cytopathic effect of mycolactone on HEK293-FRT cells was assessed after 72h of exposure, with the Alamar Blue assay (Life Technologies). Its effect on secretory protein production was assessed with the Gaussia Glow-Juice Luciferase kit (PJK GmbH), as follows. HEK293-FRT cell lines expressing wt or R66G-Sec61 $\alpha$  were grown on a 6-well plate, then transfected with a plasmid encoding a signal sequence-containing Gaussia luciferase using Fugene 6. The expression of both the luciferase and Sec61 $\alpha$  was induced 5h later by addition of doxycycline (1  $\mu$ g/ml). On the next day, cells were plated in 96-well plates (200 000 cells/well) and treated 5h later with increasing concentrations of mycolactone. Luciferase activity in culture media was measured 24h later with EnSpire Multimode Plate Reader (Perkin Elmer). Assays of mycolactone inhibition on cytokine production and homing receptors by mouse and human immune cells have been described previously (Boulkroun et al., 2010; Guenin-Mace et al., 2015; Guenin-Mace et al., 2011).

**WASP/N-WASP and AT2R silencing.** siRNAs were ON-Target plus SMARTpools (GE Healthcare Dharmacon) targeting human WASP (L-028294-00-0005), N-WASP (L-006444-00-0005), AT2R (L-005429-00-005), or non-targeting SMARTpool (D0018101005) as controls. Jurkat T cells ( $10^7$ ) were electroporated twice at 48h interval with 400 nM siRNA, using the Gene Pulser Xcell™ system (BIO-RAD) at 300 V, 500  $\mu$ F. Silencing of WASP/N-WASP expression was optimal 24h after the second

electroporation. HeLa cells were transfected with 10 nM siRNA, using Lipofectamine RNAiMAX (Invitrogen). AT2R silencing was optimal 48h post-transfection.

**Mouse studies.** Eight-week-old female mice (C57BL/6NCrI from Charles River or congenic CD45.1 (B6.SJL-*Ptprc*<sup>a</sup> *Pepc*<sup>b</sup>/BoyCrIPas) from our animal facilities) were housed under pathogen-free conditions with food and water *ad libitum*. The described experiments received the approval of the French Ministry of Higher Education and Research. They were performed in compliance with national guidelines and regulations.

**Statistical analysis.** Two group comparisons used the Mann-Whitney's rank test. Statistical analyses were performed with the *StatView*<sup>®</sup> 5 software (SAS Institute, Inc., USA) and values of  $P \leq 0.05$  were considered significant. The Prism software (5.0d; La Jolla, CA) was used for graphical representation.

**Online supplemental material.** Fig. S1: Chemical structures of all mycolactone and cotransin analogs used in this study; mapping of mycolactone-resistance mutations in a three-dimensional model of Sec61 $\alpha$  structure; IVT controls. Fig. S2: Differential cytotoxicity of mycolactone and CT8 in human fibroblasts and T lymphocytes; study of WASP/N-WASP and AT2R contribution to mycolactone-mediated inhibition of secretory protein production. Table S1: Mycolactone-susceptible proteins in Jurkat T cells, as detected by our SILAC analysis.

## ACKNOWLEDGEMENTS

We thank T. Chaze and M. Matondo-Bouzanda from the Pasteur Proteomics platform for assistance with proteome analyses. D. Tranter is acknowledged for valuable technical assistance. We are also grateful to P. Cossart and A. Echard for critical reading of the manuscript. This work was supported by the Fondation de la Recherche Médicale (FRM 2012 DEQ20120323704, C.D.), the Association Raoul Follereau (C.D.), the Région Ile de France (dim130027, C.D.), the Academy of Finland (grant 289737, V.O.P.), the Sigrid Juselius Foundation (V.O.P.) and Biocentrum Helsinki (V.O.P.). F.I. received financial support from a Pasteur-Roux Fellowship. The authors declare that they have no competing interests.

## REFERENCES

- Besemer, J., H. Harant, S. Wang, B. Oberhauser, K. Marquardt, C.A. Foster, E.P. Schreiner, J.E. de Vries, C. Dascher-Nadel, and I.J. Lindley. 2005. Selective inhibition of cotranslational translocation of vascular cell adhesion molecule 1. *Nature* 436:290-293.
- Bieri, R., M. Bolz, M.T. Ruf, and G. Pluschke. 2016. Interferon-gamma Is a Crucial Activator of Early Host Immune Defense against Mycobacterium ulcerans Infection in Mice. *PLoS Negl Trop Dis* 10:e0004450.
- Boulkroun, S., L. Guenin-Mace, M.I. Thoulouze, M. Monot, A. Merckx, G. Langsley, G. Bismuth, V. Di Bartolo, and C. Demangel. 2010. Mycolactone suppresses T cell responsiveness by altering both early signaling and posttranslational events. *J Immunol* 184:1436-1444.
- Chany, A.C., V. Casarotto, M. Schmitt, C. Tarnus, L. Guenin-Mace, C. Demangel, O. Mirguet, J. Eustache, and N. Blanchard. 2011. A diverted total synthesis of mycolactone analogues: an insight into buruli ulcer toxins. *Chemistry* 17:14413-14419.
- Cox, J., and M. Mann. 2008. MaxQuant enables high peptide identification rates, individualized p.p.b.-range mass accuracies and proteome-wide protein quantification. *Nat Biotechnol* 26:1367-1372.
- Cox, J., N. Neuhauser, A. Michalski, R.A. Scheltema, J.V. Olsen, and M. Mann. 2011. Andromeda: a peptide search engine integrated into the MaxQuant environment. *J Proteome Res* 10:1794-1805.
- Demangel, C., T.P. Stinear, and S.T. Cole. 2009. Buruli ulcer: reductive evolution enhances pathogenicity of Mycobacterium ulcerans. *Nat Rev Microbiol* 7:50-60.
- Flynn, J.L., and J. Chan. 2001. Immunology of tuberculosis. *Annu Rev Immunol* 19:93-129.
- Garrison, J.L., E.J. Kunkel, R.S. Hegde, and J. Taunton. 2005. A substrate-specific inhibitor of protein translocation into the endoplasmic reticulum. *Nature* 436:285-289.
- George, K.M., D. Chatterjee, G. Gunawardana, D. Welty, J. Hayman, R. Lee, and P.L. Small. 1999. Mycolactone: a polyketide toxin from Mycobacterium ulcerans required for virulence. *Science* 283:854-857.

- Guarner, J., J. Bartlett, E.A. Whitney, P.L. Raghunathan, Y. Stienstra, K. Asamo, S. Etuaful, E. Klutse, E. Quarshie, T.S. van der Werf, W.T. van der Graaf, C.H. King, and D.A. Ashford. 2003. Histopathologic features of *Mycobacterium ulcerans* infection. *Emerg Infect Dis* 9:651-656.
- Guenin-Mace, L., L. Baron, A.C. Chany, C. Tresse, S. Saint-Auret, F. Jonsson, F. Le Chevalier, P. Bruhns, G. Bismuth, S. Hidalgo-Lucas, J.F. Bisson, N. Blanchard, and C. Demangel. 2015. Shaping mycolactone for therapeutic use against inflammatory disorders. *Sci Transl Med* 7:289ra285.
- Guenin-Mace, L., F. Carrette, F. Asperti-Boursin, A. Le Bon, L. Caleechurn, V. Di Bartolo, A. Fontanet, G. Bismuth, and C. Demangel. 2011. Mycolactone impairs T cell homing by suppressing microRNA control of L-selectin expression. *Proc Natl Acad Sci U S A* 108:12833-12838.
- Guenin-Mace, L., R. Veyron-Churlet, M.I. Thoulouze, G. Romet-Lemonne, H. Hong, P.F. Leadlay, A. Danckaert, M.T. Ruf, S. Mostowy, C. Zurzolo, P. Bousso, F. Chretien, M.F. Carlier, and C. Demangel. 2013. Mycolactone activation of Wiskott-Aldrich syndrome proteins underpins Buruli ulcer formation. *J Clin Invest* 123:1501-12.
- Hall, B., and R. Simmonds. 2014. Pleiotropic molecular effects of the *Mycobacterium ulcerans* virulence factor mycolactone underlying the cell death and immunosuppression seen in Buruli ulcer. *Biochem Soc Trans* 42:177-183.
- Hall, B.S., K. Hill, M. McKenna, J. Ogbechi, S. High, A.E. Willis, and R.E. Simmonds. 2014. The Pathogenic Mechanism of the *Mycobacterium ulcerans* Virulence Factor, Mycolactone, Depends on Blockade of Protein Translocation into the ER. *PLoS Pathog* 10:e1004061.
- Heaton, N.S., N. Moshkina, R. Fenouil, T.J. Gardner, S. Aguirre, P.S. Shah, N. Zhao, L. Manganaro, J.F. Hultquist, J. Noel, D.H. Sachs, J. Hamilton, P.E. Leon, A. Chawdury, S. Tripathi, C. Melegari, L. Campisi, R. Hai, G. Metreveli, A.V. Gamarnik, A. Garcia-Sastre, B. Greenbaum, V. Simon, A. Fernandez-Sesma, N.J. Krogan, L.C. Mulder, H. van Bakel, D. Tortorella, J. Taunton, P. Palese, and I. Marazzi. 2016. Targeting Viral Proteostasis Limits Influenza Virus, HIV, and Dengue Virus Infection. *Immunity* 44:46-58.

- Hong, H., E. Coutanceau, M. Leclerc, L. Caleechurn, P.F. Leadlay, and C. Demangel. 2008. Mycolactone Diffuses from Mycobacterium ulcerans-Infected Tissues and Targets Mononuclear Cells in Peripheral Blood and Lymphoid Organs. *PLoS Negl Trop Dis* 2:e325.
- Huang, D.W., B.T. Sherman, and R.A. Lempicki. 2009. Systematic and integrative analysis of large gene lists using DAVID bioinformatics resources. *Nature protocols* 4:44-57.
- Junne, T., J. Wong, C. Studer, T. Aust, B.W. Bauer, M. Beibel, B. Bhullar, R. Bruccoleri, J. Eichenberger, D. Estoppey, N. Hartmann, B. Knapp, P. Krastel, N. Melin, E.J. Oakeley, L. Oberer, R. Riedl, G. Roma, S. Schuierer, F. Petersen, J.A. Tallarico, T.A. Rapoport, M. Spiess, and D. Hoepfner. 2015. Decatransin, a new natural product inhibiting protein translocation at the Sec61/SecYEG translocon. *J Cell Sci* 128:1217-1229.
- Lundin, C., H. Kim, I. Nilsson, S.H. White, and G. von Heijne. 2008. Molecular code for protein insertion in the endoplasmic reticulum membrane is similar for N(in)-C(out) and N(out)-C(in) transmembrane helices. *Proc Natl Acad Sci U S A* 105:15702-15707.
- MacKinnon, A.L., J.L. Garrison, R.S. Hegde, and J. Taunton. 2007. Photo-leucine incorporation reveals the target of a cyclodepsipeptide inhibitor of cotranslational translocation. *J Am Chem Soc* 129:14560-14561.
- Mackinnon, A.L., V.O. Paavilainen, A. Sharma, R.S. Hegde, and J. Taunton. 2014. An allosteric Sec61 inhibitor traps nascent transmembrane helices at the lateral gate. *eLife* 3:e01483.
- Maifeld, S.V., A.L. MacKinnon, J.L. Garrison, A. Sharma, E.J. Kunkel, R.S. Hegde, and J. Taunton. 2011. Secretory protein profiling reveals TNF-alpha inactivation by selective and promiscuous Sec61 modulators. *Chem Biol* 18:1082-1088.
- Marion, E., O.R. Song, T. Christophe, J. Babonneau, D. Fenistein, J. Eyer, F. Letournel, D. Henrion, N. Clere, V. Paille, N.C. Guerineau, J.P. Saint Andre, P. Gersbach, K.H. Altmann, T.P. Stinear, Y. Comoglio, G. Sandoz, L. Preisser, Y. Delneste, E. Yeramian, L. Marsollier, and P. Brodin. 2014. Mycobacterial toxin induces analgesia in buruli ulcer by targeting the Angiotensin pathways. *Cell* 157:1565-1576.
- McKenna, M., R.E. Simmonds, and S. High. 2016. Mechanistic insights into the inhibition of Sec61-dependent co- and post-translational translocation by mycolactone. *J Cell Sci* 129:1404-15.

- Monne, M., G. Gafvelin, R. Nilsson, and G. von Heijne. 1999. N-tail translocation in a eukaryotic polytopic membrane protein: synergy between neighboring transmembrane segments. *Eur J Biochem* 263:264-269.
- Paatero, A.O., J. Kellosalo, B.M. Dunyak, J. Almaliti, J.E. Gestwicki, W.H. Gerwick, J. Taunton, and V.O. Paavilainen. 2016. Apratoxin Kills Cells by Direct Blockade of the Sec61 Protein Translocation Channel. *Cell Chem Biol* 23:561-566.
- Park, E., and T.A. Rapoport. 2012. Mechanisms of Sec61/SecY-mediated protein translocation across membranes. *Annu Review Biophys* 41:21-40.
- Phillips, R., F.S. Sarfo, L. Guenin-Mace, J. Decalf, M. Wansbrough-Jones, M.L. Albert, and C. Demangel. 2009. Immunosuppressive Signature of Cutaneous Mycobacterium ulcerans Infection in the Peripheral Blood of Patients with Buruli Ulcer Disease. *J Infect Dis* 200:1675-84.
- Sarfo, F.S., F. Le Chevalier, N. Aka, R.O. Phillips, Y. Amoako, I.G. Boneca, P. Lenormand, M. Dosso, M. Wansbrough-Jones, R. Veyron-Churlet, L. Guenin-Mace, and C. Demangel. 2011. Mycolactone diffuses into the peripheral blood of buruli ulcer patients - implications for diagnosis and disease monitoring. *PLoS Negl Trop Dis* 5:e1237.
- Sharma, A., M. Mariappan, S. Appathurai, and R.S. Hegde. 2010. In vitro dissection of protein translocation into the mammalian endoplasmic reticulum. *Methods Mol Biol* 619:339-363.
- Spangenberg, T., and Y. Kishi. 2010. Highly sensitive, operationally simple, cost/time effective detection of the mycolactones from the human pathogen Mycobacterium ulcerans. *Chem Commun* 46:1410-1412.
- Walter, P., and G. Blobel. 1983. Preparation of Microsomal-Membranes for Cotranslational Protein Translocation. *Method Enzymol* 96:84-93.

## FIGURE LEGENDS

### Figure 1. Mycolactone targets the Sec61 translocon

Canine rough microsomes (CRM) were pre-incubated with increasing concentrations of mycolactone (A) or CT9 (B) at the indicated concentrations, followed by 100 nM CT7. Covalent CT7/Sec61 $\alpha$  adduct was detected using click chemistry between the alkyne group in CT7 and rhodamine-azide (TAMRA). (C) As in (A), but comparing the competitive activity of mycolactone (Myco) to that of synthetic subunits of the intact molecule. (D) CRM were incubated with a saturating concentration of mycolactone (10 $\mu$ M) either before (pre-) or after (post-) extensive washing. CT7 photocrosslinking was performed after final CRM pelleting. (E) HEK293-FRT TRex cells stably expressing wt- or mutant Sec61 $\alpha$  were treated with increasing concentrations of mycolactone for 72h and cell viability analyzed by the Alamar Blue assay (Mean  $\pm$  SEM, n=4). (F) HEK293-FRT TRex cells stably expressing wt- or R66G-Sec61 $\alpha$  were transfected for inducible expression of a secreted Gaussia luciferase then treated with increasing concentrations of mycolactone for 24h. Data are luminescence values (Mean  $\pm$  SEM, n=2) measured from culture supernatants. Data shown in Figure 1A, B, C, D, E and F are from one of two independent experiments, which gave similar results.

### Figure 2. Mycolactone is a broad-spectrum inhibitor of Sec61.

(A) Scatter plot showing the log<sub>2</sub> SILAC ratios for individual proteins quantified in analysis 1 on the X-axis (light condition: 40 nM mycolactone (Myco), heavy condition: vehicle control (Ctrl)) and analysis 2 on the Y-axis (reversed conditions). Proteins with a log<sub>2</sub> ratio <-0.5 (pink square) or >0.5 (blue square) in both analyses were considered modulated by mycolactone. GO\_CC (B) and SP-PIR keywords (C) annotation analyses of the proteins that were reproducibly down-regulated in mycolactone-exposed T cells (red; n=52), compared to “identified proteins” (blue; n=6,503) and all human proteins in UniProt (grey; n=20,204). (D) Distribution of “downregulated” (red), “identified” (blue) and “all human” proteins (grey) over different categories of membrane proteins. Statistics in (B, C, D) were calculated by Fisher Exact tests comparing “downregulated” vs. “identified” proteins; \*\*\*P<0.001. (E) *In vitro* translocation (IVT) assays of various Sec61 clients in the presence of increasing concentrations of mycolactone (Myco).

Correctly translocated protein species are indicated with arrowheads and protease-resistant fragments, or non-translocated protein species with asterisks. ER translocation of non-glycosylated proteins (prolactin, IFN- $\gamma$  and BiP) was assessed by treatment with proteinase K (PK), with resistance to PK indicating correct translocation into the ER lumen. Detergent-treated controls are shown in Fig. S1C. It should be noted that BiP is largely protease-resistant and upon PK treatment forms shorter fragments. Translocation of glycosylated proteins (Mcln, LEP and CIG30) was assessed by analyzing the change in migration in SDS-PAGE and autoradiography. Glycosidase-treated controls are shown in Fig. S1C. Data shown in Fig. 2E are from one of two independent experiments, which gave similar results.

**Figure 3. Mycolactone targets primarily the IFN- $\gamma$  signaling pathway in Jurkat T cells.**

(A) Production of IFN- $\gamma$  by Jurkat T cells treated with 20 nM Mycolactone (Myco) or vehicle (Ctrl) for 6h (Resting), or for 1h prior to 6h of activation with PMA/IO. (B) Quantitation of *IFN- $\gamma$*  mRNAs in Jurkat T cells treated with mycolactone (Myco) or vehicle (Ctrl) for 6h (Resting) or for 1h prior to 3 or 6h of activation with PMA/IO. (C) Western blot analysis of tyrosine phosphorylated (STAT1-P) and total STAT1 in Jurkat T cells treated with mycolactone (Myco) or vehicle (Ctrl) for the indicated times prior to activation with 1 ng/ml IFN- $\gamma$  for 20 min, or left unstimulated (Unst). (D) Flow cytometric analysis of surface expression of IFNGR1, IFNAR1 and IFNAR2 by Jurkat T cells incubated with or without mycolactone for 6h. (E) Quantification of *IFNGR1* mRNAs in Jurkat T cells treated as in (B). Quantitation of *GBP2* mRNAs (F) and total GBP2 protein (G) in Jurkat T cells treated as in (B). (H) Western blot analysis of phosphorylated (-P) and total STAT1, STAT2, STAT3 and  $\beta$ -actin as loading control, in Jurkat T cells treated with mycolactone (Myco) or vehicle (Ctrl) for 24h prior to activation with 1 ng/ml IFN- $\gamma$  or IFN- $\alpha$  for 20 min, or left unstimulated (Unst). Data in (B,E,F) are mean fold changes  $\pm$  SEM of one experiment performed in duplicate, compared to resting controls, while those in (D) are mean MFI  $\pm$  SEM of one experiment performed in triplicate, relative to vehicle controls. Similar results were obtained in independent experiments. Data in (A,C,G,H) are from one of two independent experiments, which gave similar results.

**Figure 4. The R66G mutation in Sec61 $\alpha$  confers resistance to mycolactone**

(A) Primary mouse T cells were activated with anti-CD3/CD28 antibodies, then transduced with wt- or R66G-Sec61 $\alpha$  prior to exposure to mycolactone, in resting or PMA/IO-stimulated conditions. (B) Differential effect of mycolactone (24h, 400 nM) on the CD4 surface expression of wt- or R66G-Sec61 $\alpha$  transduced (Zsgreen<sup>+</sup>) cells. Data are MFI from one of two independent experiments, which gave similar results. (C) Dose-dependent effect of mycolactone on the CD62L surface expression of wt- or R66G-Sec61 $\alpha$  transduced (Zsgreen<sup>+</sup>-gated) cells. (D) Effect of a 1h pre-treatment with increasing doses of mycolactone on the PMA/IO-induced production of IFN- $\gamma$  by primary T cells transduced with wt- or R66G-Sec61 $\alpha$  (Zsgreen<sup>+</sup>-gated) cells. (E) Bone marrow-derived macrophages were transduced with wt- or R66G-Sec61 $\alpha$  prior to exposure to mycolactone, in resting or LPS+IFN- $\gamma$ -stimulated conditions. (F) Dose-dependent effect of mycolactone on the IFNGR1 surface expression of wt- or R66G-Sec61 $\alpha$  transduced (Zsgreen<sup>+</sup>-gated) cells. (G) Dose-dependent effect of mycolactone on the LPS/FN- $\gamma$ -induced production of iNOS by wt- or R66G-Sec61 $\alpha$  transduced (Zsgreen<sup>+</sup>-gated) cells. Data in C,D,F,G are MFI or mean cell percentages +/- SEM of triplicates, relative to vehicle controls (Ctrl). They are from one of two independent experiments, which gave similar results.

**Figure 5. Mycolactone suppresses Sec61 activity in T cells *in vivo***

(A) Primary T cells isolated from wild-type (C57BL/6J, CD45.2<sup>+</sup>) and congenic CD45.1 mice were transduced with wt- or R66G-Sec61 $\alpha$  and mixed, as described. Each cell mix was injected intravenously into 4 recipient mice, 2 of which received concomitantly an intraperitoneal injection of mycolactone, and the other 2 vehicle as control. (B) CD62L surface expression on wt- and R66-Sec61 $\alpha$  T cells (CD45.1<sup>+</sup>- or CD45.1<sup>-</sup>, Zsgreen<sup>+</sup>-gated) recovered from spleen and PLN. (C) Relative proportion of R66G-Sec61 $\alpha$  cells, compared to wt-Sec61 $\alpha$  cells, in spleen and PLN. Data are MFI (B) and mean cell numbers (C) in each experimental group, presented as box and whiskers (\*P $\leq$ 0.05, Mann-Whitney, each box corresponding to 4 experimental values). They are representative of two independent experiments giving similar results.

## SUPPLEMENTAL LEGENDS

**Figure S1.** (A) Chemical structures of natural mycolactone (A/B form, from *M. ulcerans* strain 1615), synthetic subunits of mycolactone and cotransin variants used in this study. (B) Mutations associated with mycolactone resistance are located near the luminal plug of Sec61 $\alpha$ . Homology model of human Sec61 $\alpha$ , showing the location of mycolactone-resistance mutations (red). Lateral gate helices (hydrophobic transmembrane domains TM2/3 and TM7/8) are colored in blue and green, respectively. (C) ER translocation of BiP, prolactin and IFN- $\gamma$  were confirmed by proteinase K (PK) treatment in the presence and absence of detergent (TX-100). Correctly translocated protein species are indicated with arrowheads. Protease-resistant fragments are indicated with asterisks. ER translocation of these non-glycosylated proteins does not cause a change in band mobility, and resistance to PK was used to indicate the fraction of ER translocated polypeptide. Treating microsomes with PK and detergent abolished the protected species, indicating correct translocation to the lumen of ER microsomes. Glycosylation of CIG30 and LEP was assessed by Endoglycosidase H (EndoH) treatment. Membrane-integrated, glycosylated protein species are indicated with arrowheads and non-integrated species with an asterisk. Difference in band mobility indicates that these proteins become glycosylated within the ER lumen upon correct membrane integration. Endoglycosidase H (EndoH) treatment demonstrates that the altered mobility is due to protein glycosylation.

**Figure S2.** (A) Differential cytotoxicity of mycolactone and CT8. (Left) Cell viability, as assessed by methylthiazolyl-tetrazolium (MTT) reduction, of human primary dermal fibroblasts (HDF) incubated with mycolactone, CT8 or solvent for 72 hours. (Right) Induction of apoptosis in Jurkat T cells incubated with mycolactone, CT8 or solvent for 48 hours. Annexin V<sup>+</sup>/propidium iodide (PI)<sup>-</sup> cells were identified as early apoptotic cells, Annexin V<sup>+</sup>/PI<sup>+</sup> cells as late apoptotic (dead) cells, and Annexin V<sup>-</sup>/PI<sup>-</sup> cells as live cells. Data are mean percentages  $\pm$  SD of duplicates relative to solvent, and are representative of three independent experiments. (B) Mycolactone-mediated inhibition of secreted and membrane protein production is WASP/N-WASP-independent. Western blot analysis of total WASP, N-WASP, and GAPDH as

loading control, in Jurkat T cells transfected with siRNAs targeting WASP, N-WASP, both proteins or non-targeting siRNAs as controls (NT) for 48h. (Left) Flow cytometric analysis of CD62L surface expression in siRNA-transfected Jurkat T cells exposed to 25 nM mycolactone (Myco) or solvent (Ctrl) for 16h. Mean fluorescent intensities (MFI)  $\pm$  SD of duplicates. (Right) IL-2 production by siRNA-transfected Jurkat T cells treated with 25 nM mycolactone (Myco) or solvent (Ctrl) for 1h prior to activation with PMA/IO for 16h. Mean optical density (OD)  $\pm$  SD of duplicates. Data are representative of two independent experiments. (C) Mycolactone-mediated inhibition of secretory protein production is AT2R-independent. Western blot analysis of total AT2R, and GAPDH as loading control in HeLa cells transfected with siRNAs targeting AT2R or non-targeting siRNAs as controls (NT) for 60h, then incubated with 50 nM mycolactone or solvent for 16h. (Left) Flow cytometric analysis of IFNGR1 surface expression in siRNA-transfected HeLa cells exposed to 50 nM mycolactone (Myco) or solvent (Ctrl) for 16h. Mean fluorescent intensities (MFI). (Right) MCP-1 production by siRNA-transfected HeLa cells treated with 50 nM mycolactone (Myco) or solvent (Ctrl) for 16h. Mean optical density (OD)  $\pm$  SD of duplicates. Data are representative of two independent experiments.

**Table S1.** Proteomic profiling of mycolactone-exposed Jurkat T cells. Proteins that were downregulated (upper box) or upregulated (lower box) by mycolactone treatment are shown. Those induced by IFN- $\gamma$  are grey-shaded.

Accession <sup>a</sup>	Gene <sup>a</sup>	Full protein name <sup>a</sup>	Mean <sup>b</sup>	SD <sup>b</sup>	GO_CC <sup>a</sup>	SS or TMD <sup>c</sup>	Protein type <sup>d</sup>	IFN- $\gamma$ induced <sup>e</sup>
Q96PP8	GBP5	Guanylate-binding protein 5	-2,76	0,75	Cytoplasm, membrane			+
Q07108	CD69	Early activation antigen CD69	-2,90	0,47	Plasma membrane	TMD	SP II	-
P13746	HLA-A	HLA class I histocompatibility antigen, A-11 alpha chain	-1,91	0,84	ER, Golgi, Plasma membrane	SS	SP I	+
P32456	GBP2	Interferon-induced guanylate-binding protein 2	-2,29	0,06	Cytoplasm, Nucleus, Golgi			+
P10321	HLA-C	HLA class I histocompatibility antigen, Cw-7 alpha chain	-2,12	0,10	ER, Golgi, Plasma membrane	SS	SP I	+
Q95727	CRTAM	Cytotoxic and regulatory T-cell molecule	-2,79	1,35	Plasma membrane	SS	SP I	-
Q92854	SEMA4D	Semaphorin-4D	-1,68	0,19	Plasma membrane	SS	SP I	-
P42224	STAT1	HUMAN Signal transducer and activator of transcription 1-alpha/beta	-1,70	0,03	Cytoplasm, Nucleus			+
P01850	TRBC1	T-cell receptor beta-1 chain C region	-1,47	0,34	Plasma membrane	TMD	SP	-
P61769	B2M	Beta-2-microglobulin	-1,55	0,14	Secreted	SS		+
O43736	ITM2A	Integral membrane protein 2A	-1,56	0,05	Membrane	TMD	SP II	-
P09693	CD3G	T-cell surface glycoprotein CD3 gamma chain	-1,30	0,36	Plasma membrane	SS	SP I	-
P01737	TCRA	T-cell receptor alpha chain V region PY14	-1,39	0,17	Plasma membrane	SS		-
P04234	CD3D	T-cell surface glycoprotein CD3 delta chain	-1,29	0,02	Plasma membrane	SS	SP I	-
P32455	GBP1	Interferon-induced guanylate-binding protein 1	-1,37	0,21	Cytoplasm, Golgi, Secreted			+
P27701	CD82	CD82 antigen	-0,90	0,35	Plasma membrane	TMD	MP	-
O94901	SUN1	SUN domain-containing protein 1	-1,02	0,18	Nucleus membrane	TMD	SP II	-
Q8TDB6	DTX3L	E3 ubiquitin-protein ligase DTX3L	-1,06	0,08	Cytoplasm, Nucleus			+
P04439	HLA-A	HLA class I histocompatibility antigen, A-3 alpha chain	-1,12	0,11	Plasma membrane	SS	SP I	+
Q8IXQ6	PARP9	Poly [ADP-ribose] polymerase 9	-1,17	0,20	Cytoplasm, Nucleus			+
Q03518	TAP1	Antigen peptide transporter 1	-1,20	0,25	ER, Membrane	TMD	MP	-
P42892	ECE1	Endothelin-converting enzyme 1	-1,09	0,16	Plasma membrane	TMD	SP II	-
O75787	ATP6AP2	Renin receptor	-0,99	0,03	Plasma membrane	SS	SP I	-
P13598	ICAM2	Intercellular adhesion molecule 2	-0,92	0,06	Plasma membrane	SS	SP I	-
P43489	TNFRSF4	Tumor necrosis factor receptor superfamily member 4	-1,35	0,65	Plasma membrane	SS	SP I	-
P30533	LRPAP1	Alpha-2-macroglobulin receptor-associated protein	-0,89	0,00	ER, Cytoplasm	SS		-
Q9BQE5	APOL2	Apolipoprotein L2	-0,88	0,00	Cytoplasm			-
Q15904	ATP6AP1	V-type proton ATPase subunit S1	-0,75	0,13	Membrane, Vacuole	SS	SP	-
O14672	ADAM10	Disintegrin and metalloproteinase domain-containing protein 10	-0,87	0,04	Plasma membrane	SS	SP I	-
P11021	HSPA5 (BIP)	78 kDa glucose-regulated protein	-0,76	0,07	ER lumen	SS		-
O75976	CPD	Carboxypeptidase D	-0,84	0,10	Membrane	SS	SP I	-
P48723	HSPA13	Heat shock 70 kDa protein 13	-0,90	0,19	ER	SS		-
Q460N5	PARP14	Poly [ADP-ribose] polymerase 14	-0,67	0,08	Nucleus, Cytoplasm			-
O95399	UTS2	Urotensin-2	-0,74	0,04	Secreted	SS		-
Q96JJ7	TMX3	Protein disulfide-isomerase TMX3	-0,74	0,04	ER	SS	SP	-
P07766	CD3E	T-cell surface glycoprotein CD3 epsilon chain	-0,68	0,02	Plasma membrane	SS	SP I	-
P06127	CD5	T-cell surface glycoprotein CD5	-0,71	0,05	Plasma membrane	SS	SP I	-
Q13217	DNAJC3	DnaJ homolog subfamily C member 3	-0,59	0,08	ER	SS		-
Q8NHV1	GIMAP7	GTPase IMAP family member 7	-0,58	0,04	Lipid droplet, Cytoplasm			-
Q6PIU2	NCEH1	Neutral cholesterol ester hydrolase 1	-0,64	0,05	Membrane	TMD	SP II	-
Q9UBV2	SEL1L	Protein sel-1 homolog 1	-0,59	0,02	ER	SS	SP I	-
P20645	M6PR	Cation-dependent mannose-6-phosphate receptor	-0,60	0,00	Membrane	SS		-
Q4G148	GXYLT1	Glucoside xylosyltransferase 1	-0,62	0,07	Membrane	TMD	SP II	-
Q99805	TM9SF2	Transmembrane 9 superfamily member 2	-0,57	0,01	Endosome, Membrane	SS	MP	-
Q99519	NEU1	Sialidase-1	-0,74	0,26	Membrane	SS	MP	-
Q8NFK8	TOR1AIP2	Torsin-1A-interacting protein 2	-0,69	0,18	ER	TMD	SP	-
P09326	CD48	CD48 antigen	-0,81	0,36	Plasma membrane	SS		-
P19474	TRIM21	E3 ubiquitin-protein ligase TRIM21	-0,62	0,10	Cytoplasm, Nucleus			+
P80303	NUCB2	Nucleobindin-2	-0,54	0,00	Golgi, Membrane, ER, Nucleus	SS	MP	-
Q13308	PTK7	Inactive tyrosine-protein kinase 7	-0,59	0,07	Membrane	SS	SP I	-
Q03519	TAP2	Antigen peptide transporter 2	-0,58	0,10	ER, Membrane	TMD	MP	-
P05107	ITGB2	Integrin beta-2	-0,51	0,00	Plasma membrane	SS	SP I	-
Q96CX6	LRRCS8	Leucine-rich repeat-containing protein 58	1,28	1,04	Unknown			-
P08107	HSPA1A	Heat shock 70 kDa protein 1A/1B	0,91	0,11	Cytoplasm			-

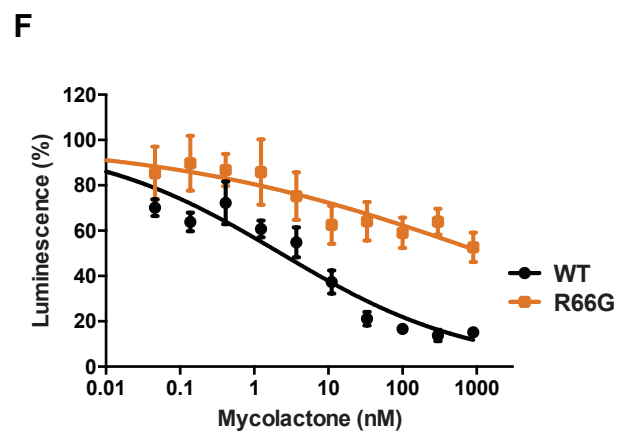
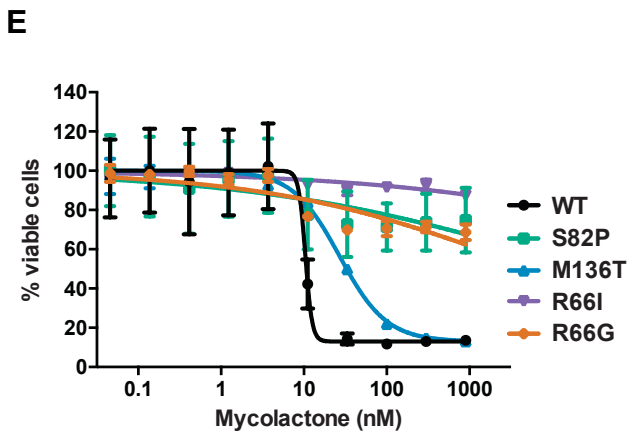
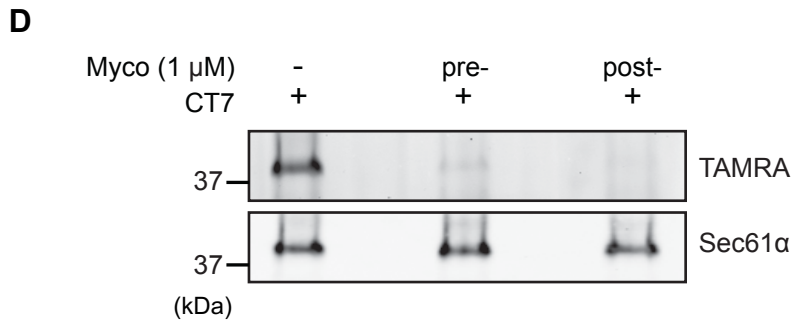
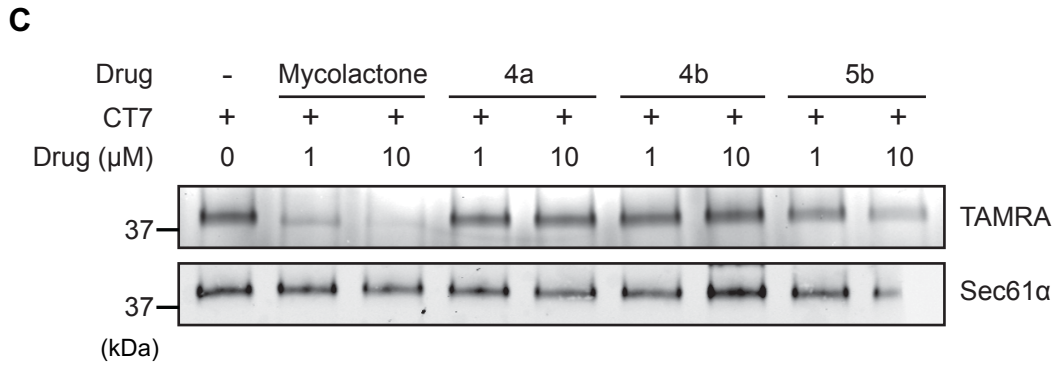
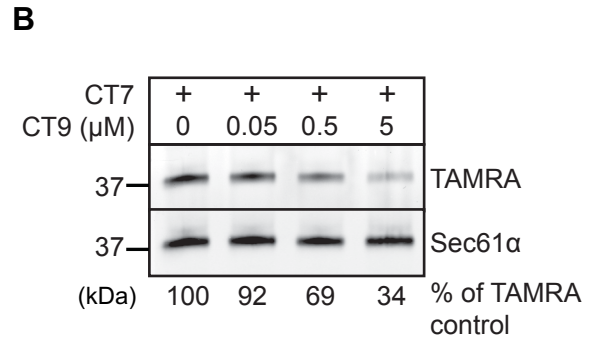
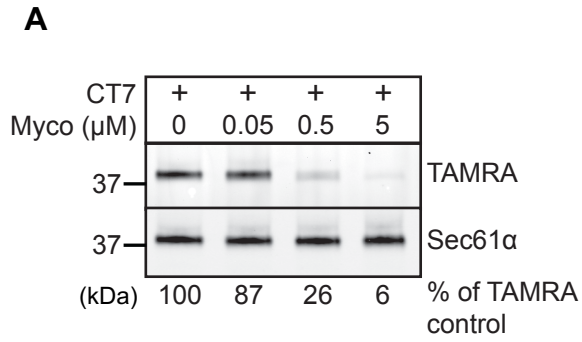
<sup>a</sup> According to [www.uniprot.org](http://www.uniprot.org)

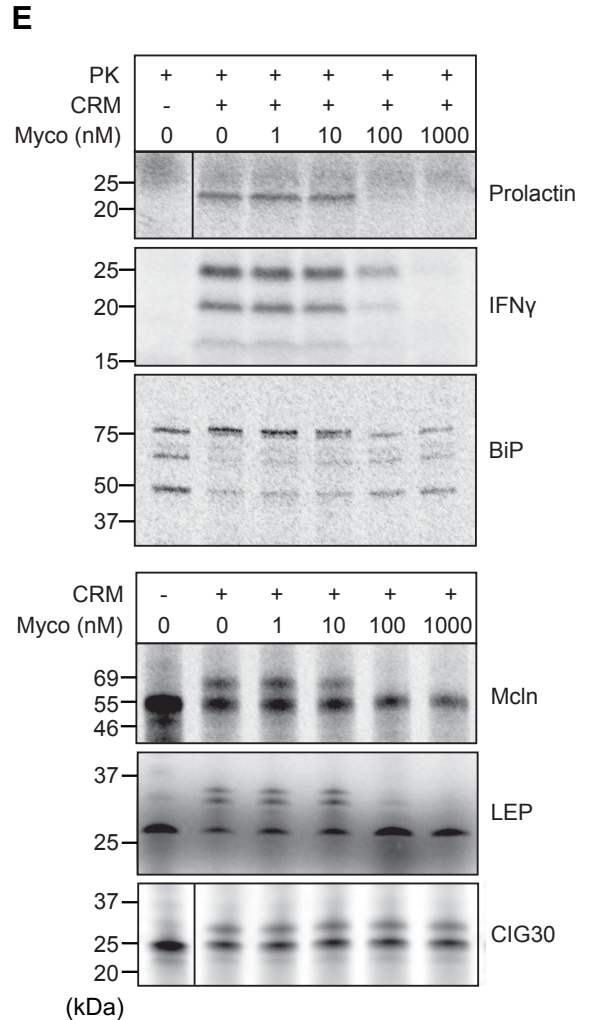
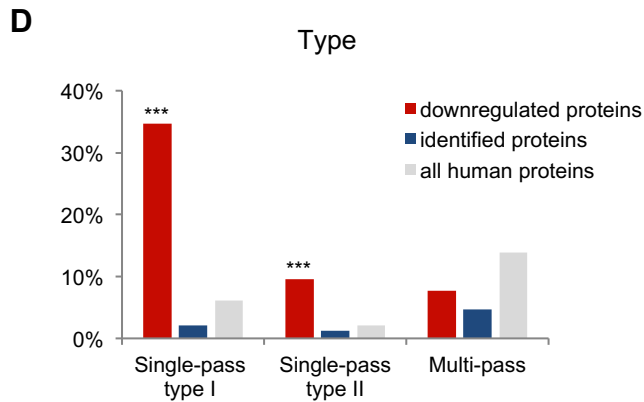
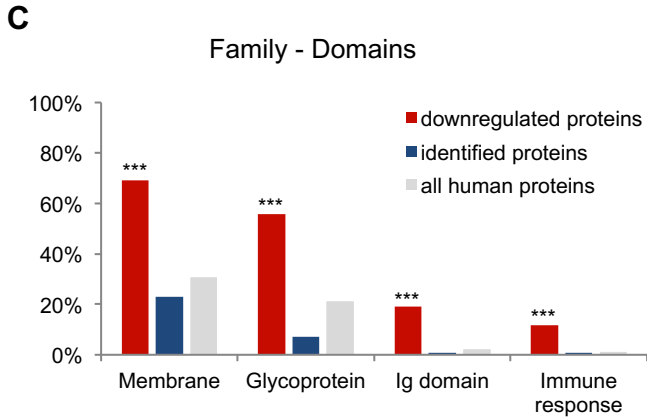
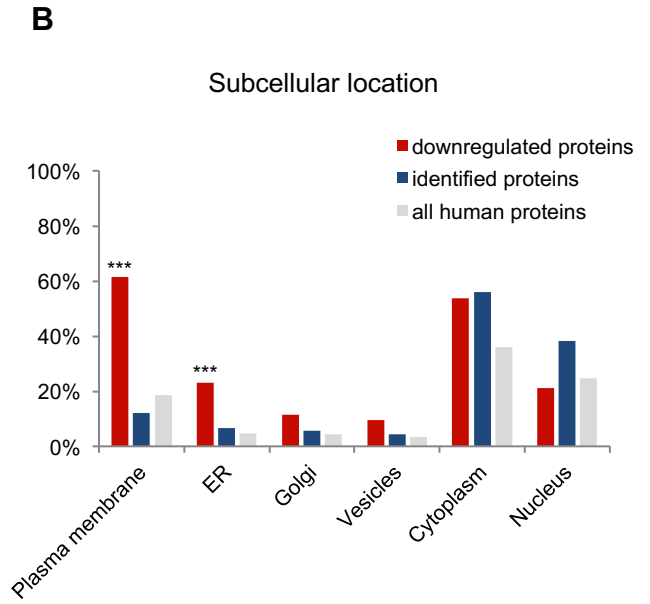
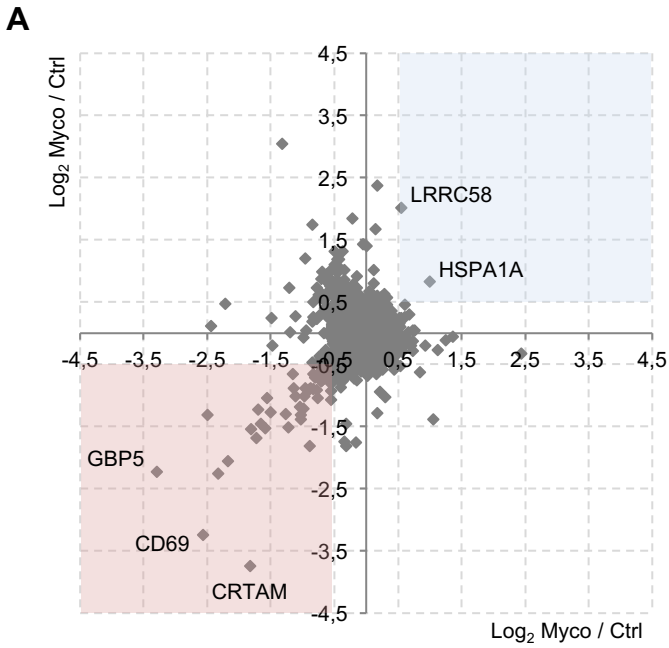
<sup>b</sup> Mean and SD of log<sub>2</sub> Myco/Ctrl ratios from two SILAC experiments

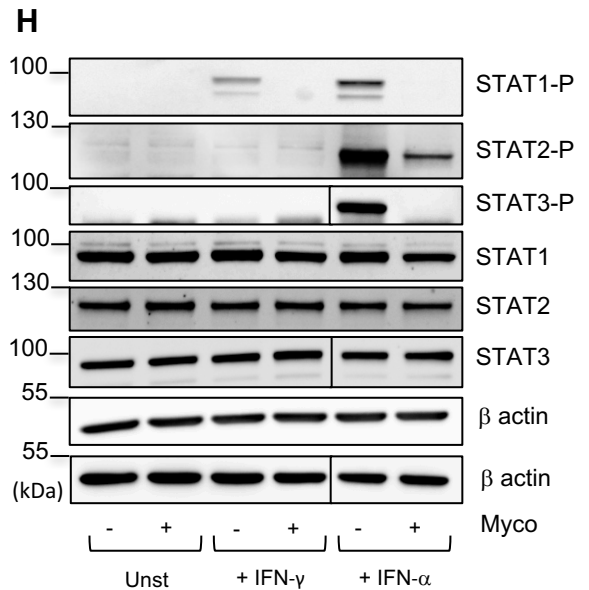
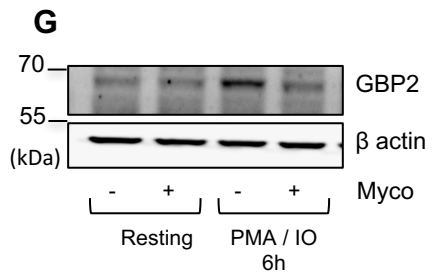
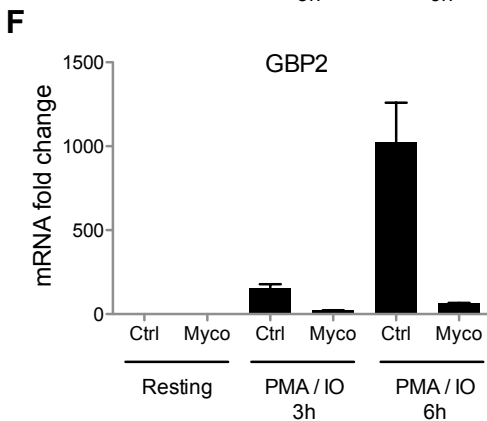
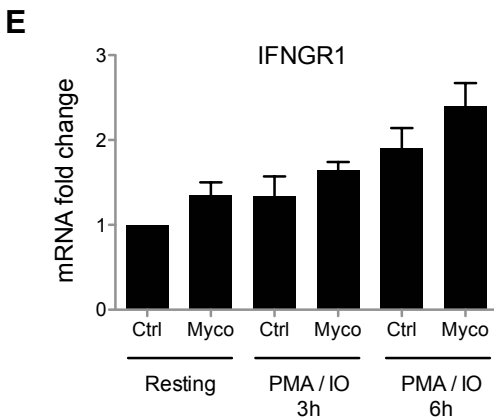
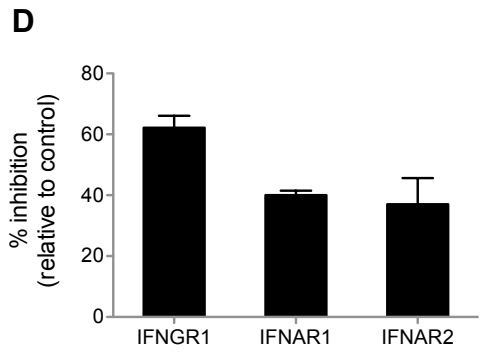
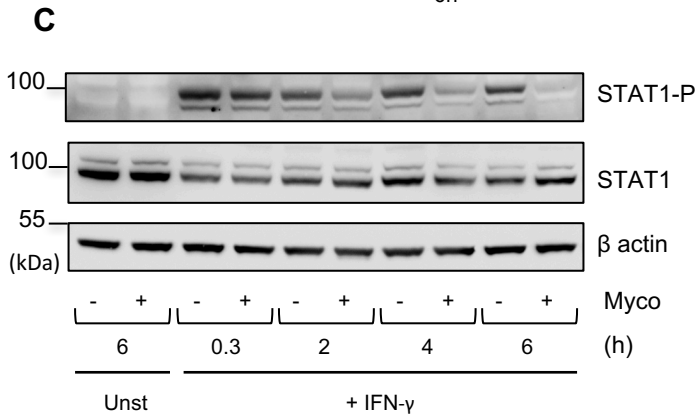
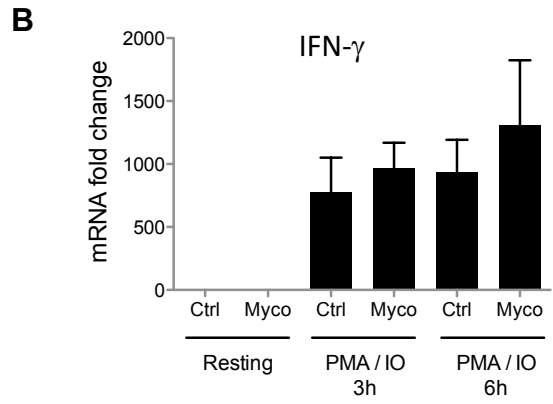
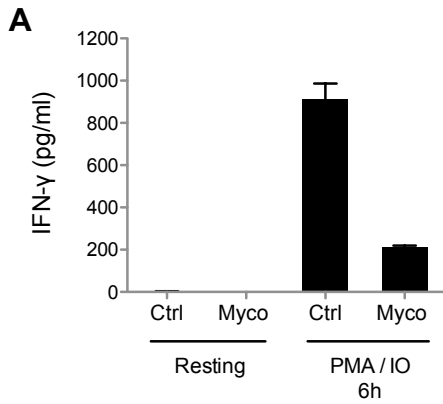
<sup>c</sup> Signal sequence (SS), transmembrane domain (TMD)

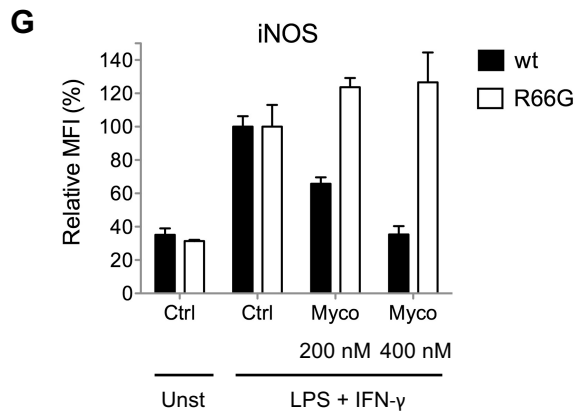
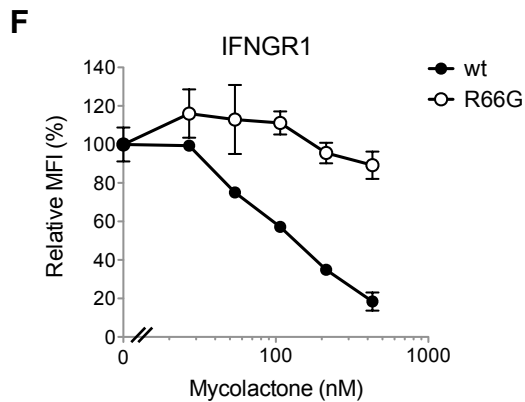
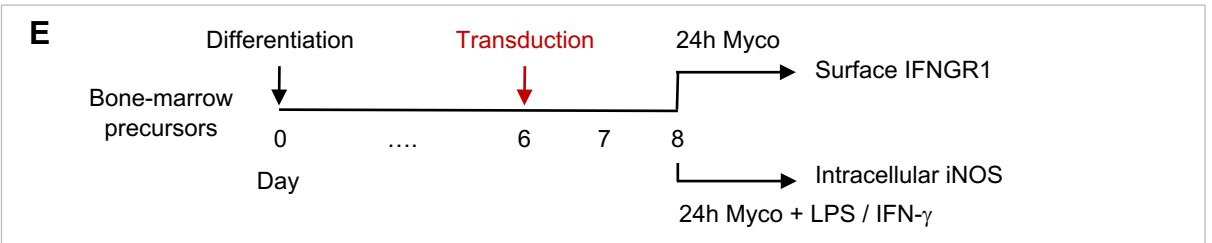
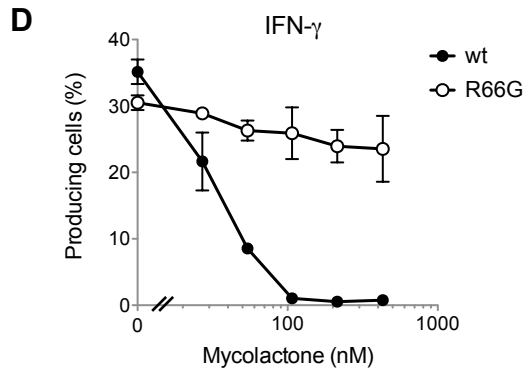
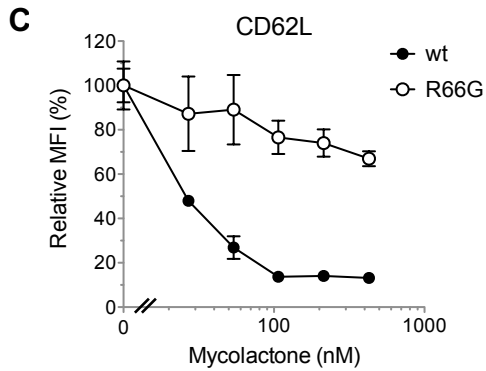
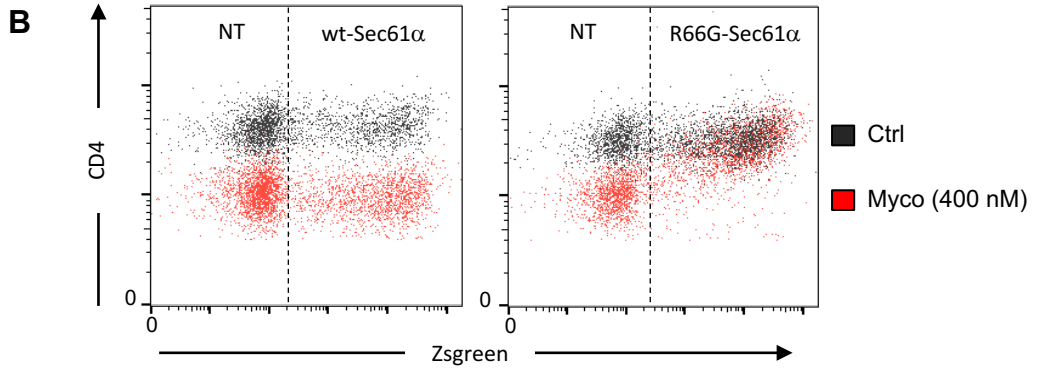
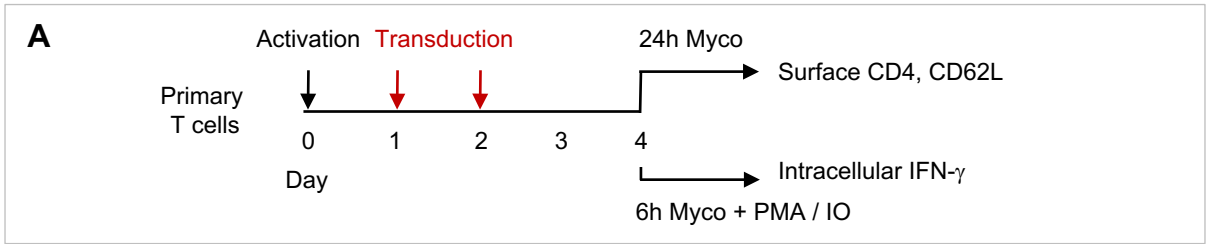
<sup>d</sup> Single Pass-Type I (SP I), Single Pass-Type II (SP II) or Multi Pass (MP)

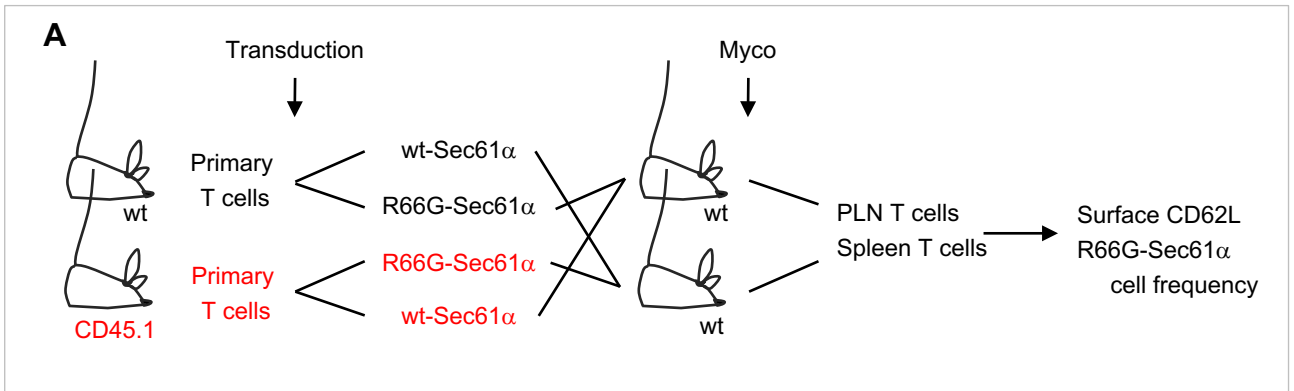
<sup>e</sup> Induced by IFN- $\gamma$  (+) or not (-), according to [www.interferome.org](http://www.interferome.org)



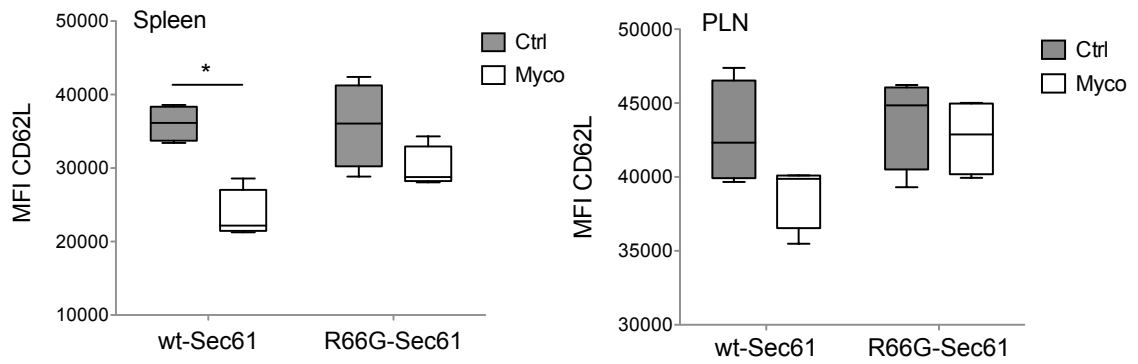




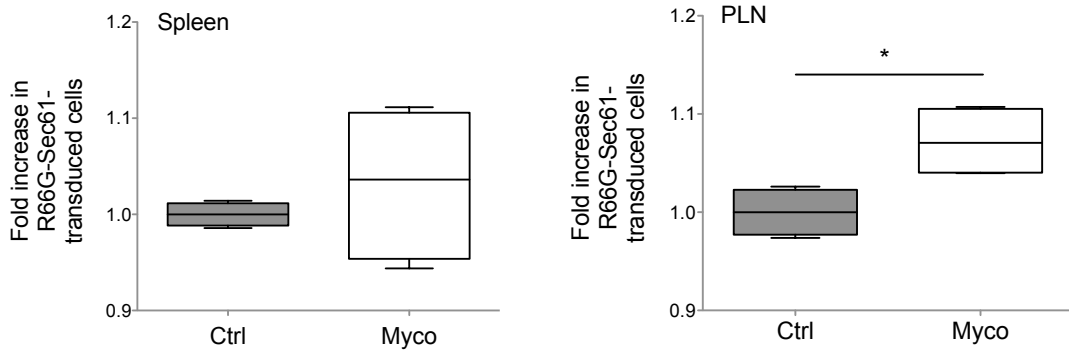


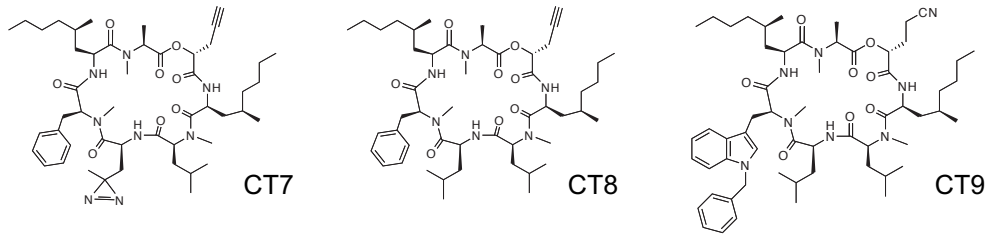
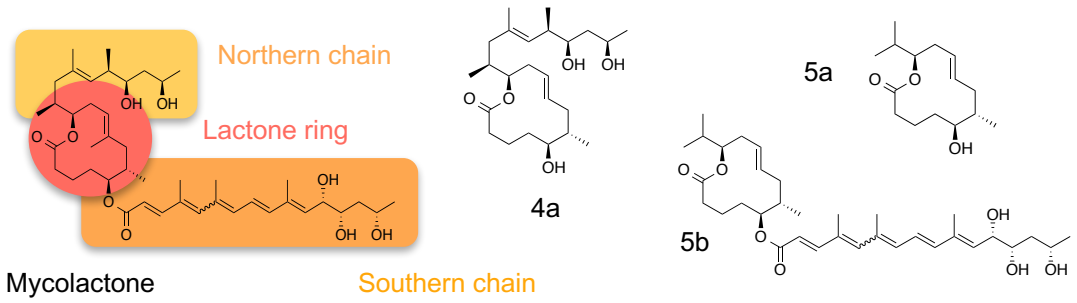
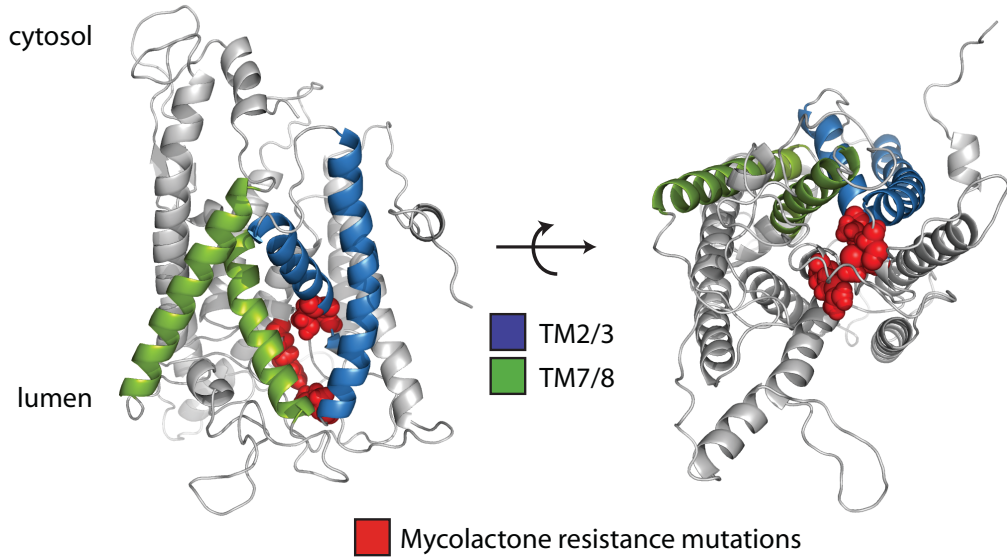
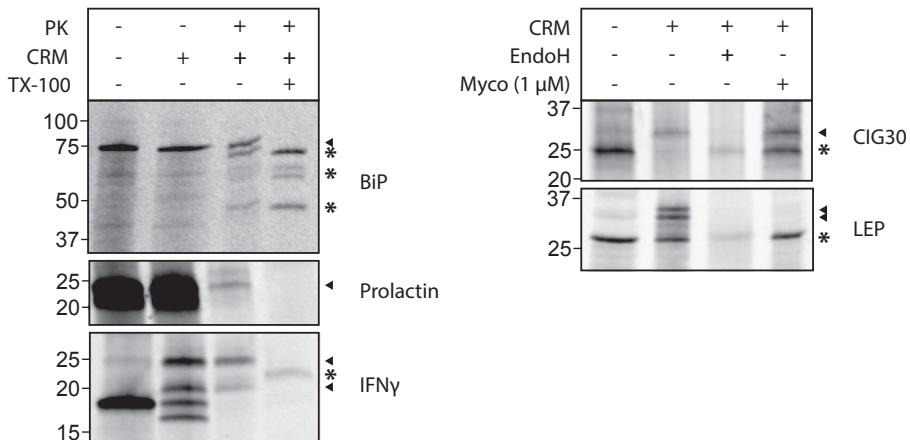


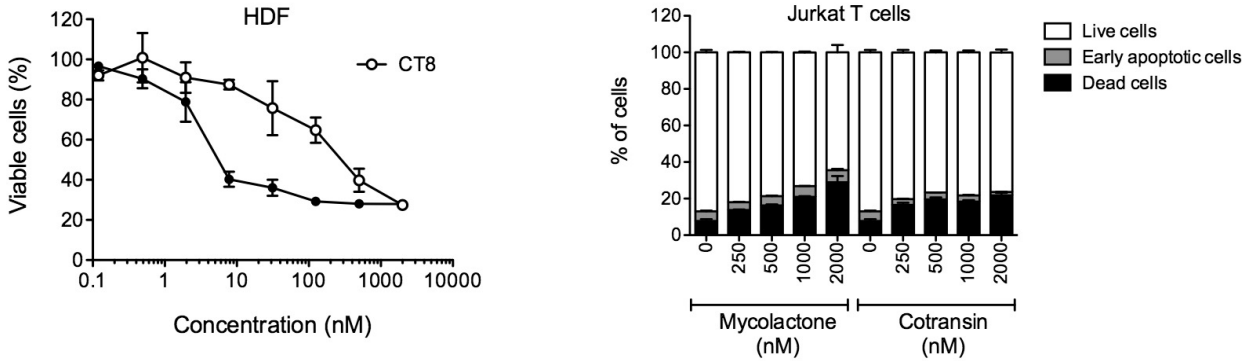
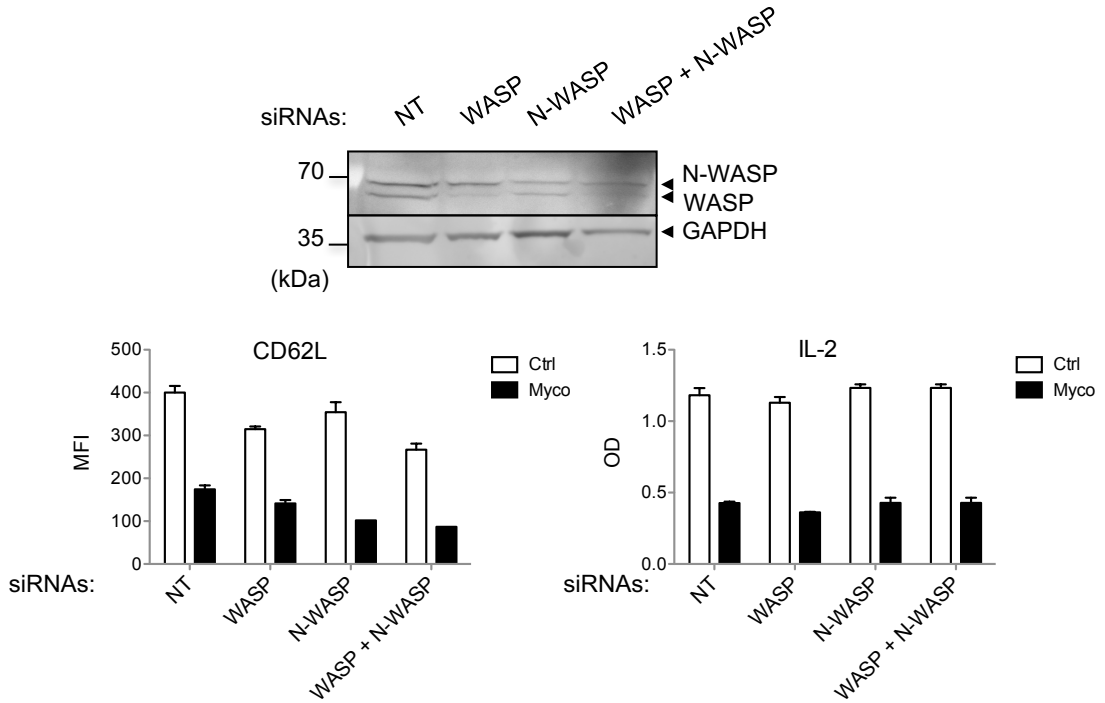
**B**



**C**



**A****B****C**

**A****B****C**